VYSOKÉ UČENÍ TECHNICKÉ V BRNĚ

BRNO UNIVERSITY OF TECHNOLOGY

FAKULTA STROJNÍHO INŽENÝRSTVÍ

FACULTY OF MECHANICAL ENGINEERING

ÚSTAV AUTOMOBILNÍHO A DOPRAVNÍHO INŽENÝRSTVÍ

INSTITUTE OF AUTOMOTIVE ENGINEERING

Měření rychlosti metodou žhavených drátků

Fluid velocity measurement by hot-wire anemometry

BAKALÁŘSKÁ PRÁCE

BACHELOR THESIS

AUTOR PRÁCE — Mohammad Abu Asad

AUTHOR

VEDOUCÍ PRÁCE — doc. Ing. František Lízal, Ph.D.

SUPERVISOR

BRNO 2022

BRNO UNIVERSITY OF TECHNOLOGY
FACULTY OF MECHANICAL ENGINEERING

Assignment Bachelor's Thesis

Institut:	Institute of Automotive Engineering
Student:	**Mohammad Sultan Abu Asad**
Degree programm:	Engineering
Branch:	Machine and Equipment Construction
Supervisor:	**doc. Ing. František Lízal, Ph.D.**
Academic year:	2021/22

As provided for by the Act No. 111/98 Coll. on higher education institutions and the BUT Study and Examination Regulations, the director of the Institute hereby assigns the following topic of Bachelor's Thesis:

Velocity measurement by hot–wire anemometry

Brief Description:

Hot–wire anemometry is one of the best methods for the measurement of the velocity of gases and liquids. This method is reliable and excels in the measurement of high–frequency velocity fluctuations and turbulence. The thesis will focus on calibration techniques for low velocities and also on techniques for measurement of turbulence downstream of wire meshes.

Bachelor's Thesis goals:

Describe principles of thermoanemometry, evaluate advantages and disadvantages in comparison with competing methods.
Perform a literature survey of methods for low–velocity calibration; identify the main problems and issues during low–velocity calibration.
Design and assemble a device for low–velocity calibration.
Perform the calibration and compare the precision of the newly designed calibrator in comparison with the standard calibrator.

Recommended bibliography:

BRUUN, H. Hot-Wire Anemometry: Principles and Signal Analysis, Oxford, Oxford University Press, 1995. 507 s. |SBN 0-19-856342-6.

JORGENSEN, F. How to measure turbulence with hot-wire anemometers: a practical guide. 1st edition. [s,l.] : Dantec Dynamics A/S, 2001. 56 s.

PAVELEK, M., ŠTĚTINA, J.: Experimentální metody v technice prostředí . Skripta. VUT Brno, 2007.

Deadline for submission Bachelor's Thesis is given by the Schedule of the Academic year 2021/22

In Brno,

L. S.

prof. Ing. Josef Štětina, Ph.D. Director of the Institute	doc. Ing. Jaroslav Katolický, Ph.D. FME dean

ABSTRAKT

Měření žhaveným drátkem o nízké rychlosti proudění obsahuje mnoho problémů, které způsobují nejistoty měření. Tato bakalářská práce se zaměřuje na tento typ měření s ohledem na práce jiných výzkumníků a poskytuje přehled teorie kalibrace žhavených drátků pro nízké rychlosti proudění. Uvádí jednoduchou alternativu k běžnému kalibrátoru od DANTEC a následně ji porovnává s laserovým Dopplerovským měřením.

KLÍČOVÁ SLOVA

Žhavené drátky, Laserová Dopplerovská anemometrie (LDA), nízké rychlosti

ABSTRACT

Hot wire measurement of low velocity is associated with several difficulties which result in a great uncertainty of measurement, this bachelor thesis focuses on such measurement with a view to other researchers' work and some scientific background about the topic and offers a simple alternative to a common calibrator from DANTEC and then compares it with laser Doppler measurement.

KEYWORDS

Hot wire anemometer (HWA); Low velocity; Laser Doppler anemometer (LDA); Constant Temperature Anemometer (CTA).

BIBLIOGRAFICKÁ CITACE

ABU ASAD, M. *Měření rychlosti metodou žhavených drátků*. Brno, 2022. Bakalářská práce. Vysoké učení technické v Brně, Fakulta strojního inženýrství, Ústav automobilního a dopravního inženýrství. Vedoucí bakalářské práce František Lízal. Dostupné také z: https://www.vutbr.cz/studenti/zav-prace/detail/140717.

ČESTNÉ PROHLÁŠENÍ

Prohlašuji, že tato práce je mým původním dílem, zpracoval jsem ji samostatně pod vedením Františka Lízala a s použitím informačních zdrojů uvedených v seznamu.

V Brně dne 10. května 2022 ……..……..……..

Mohammad Abu Asad

GRATITUDE

I would like to thank my supervisor doc. Ing. František Lízal, Ph.D., for the great help, guidance, and advice he had provided throughout my work on this thesis. I would also like to thank Ing. Ondřej Cejpek for his assistance and guidance in the laser Doppler lab.

CONTENT

1 INTRODUCTION

1.1 GENERAL OVERVIEW

Hot-wire anemometry is a well-established technique, used to acquire time-resolved measurements of fluid velocity [1,2]. The sensors are usually metal wires with diameters in the range of 2–15μm. The filament is heated by an electric current and cooled using the incident flow. The recorded wire voltage is then associated with the convective heat transfer from the wire. These results are sensitive to both velocity and the temperature of the flow [3].

Historically, hot-wires have in many instances been used in nominally steady temperature flows, at a noticeably low Mach number [4]. High-speed, high-temperature flows impose additional requirements than the ones for low Mach and low-temperature flows. Firstly, the probe material should be able to withstand the temperature as well as the mechanical stress of a hot, high-speed flow. The thin wire filament and its mechanical attachment are delicate, and frequently sustain damage when exposed to high-speed air. Secondly, high Mach number flows usually have a large fluctuation in average temperature across the flow field. While there are popular methods to account for small temperature variations, these generally require less than 20 K between the calibration temperature of the hot-wire and the drift temperature where the hot-wire is utilized [3]. On the other hand, low velocity flows also have their own complications, since the signal that hot-wire reads is relatively low and has fluctuations and many minor factors must be taken into consideration as well as sensitivity of the device itself. That's the main motivation of this thesis, to measure low velocities 0.02 – 0.5 m/s with hot-wire.

1.2 WORKING PRINCIPLE

In the one-dimensional constant temperature method, which is focused on in this thesis a thin probe is used as a resistor in the Wheatstone bridge circuit which is shown in figure (1). The circuit consists of two fixed and known resistors $R_1$and R_2 and a third one that is variable R_3. The probe is the fourth resistance R_w that completes the bridge. For the bridge to be balanced, then the following equation should apply $\frac{R_1}{R_w} = \frac{R_2}{R3}$, resulting in voltage difference equal zero (so-called error voltage). The wire resistance is a function of temperature; hence the constant temperature circuit takes use of it. The principle is the following: once the wire temperature and resistance have reached a certain working point, the variable resistor R_3 maybe changed to balance the bridge. The temperature of the wire fluctuates as the fluid velocity changes, as does the resistance. The bridge becomes imbalanced because of this impact, resulting in a voltage difference. This difference is detected by the amplifier. It re-balances the bridge by adjusting the feedback current to maintain the wire temperature and resistance constant. These variations in current may be detected and utilized to compute the flow velocity [2].

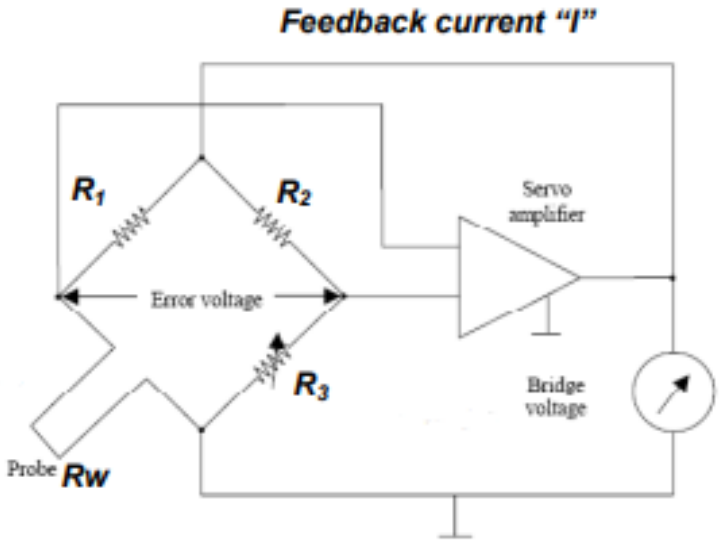

Figure 1. Wheatstone bridge circuit [2].

The heat balance equation for the wire filament must be solved to understand the link between current (often recorded as voltage reading) and flow velocity. Only the steady-state conditions will be studied to make the analysis uncomplicated. For the wire filament, the general heat balance equation is:

$$Q_g = Q_T + Q_A \qquad (2)$$

Where $Q_g$is the generated heat, $Q_T$is the heat transferred, $Q_A$is the accumulated heat. Because there is no heat accumulation Q_A in the wire at a steady state, this term equals 0. The amount of heat generated by joule heating, Q_g, is proportional to the electrical power applied to the wire. It is defined as follows:

$$Q_g = I^2 R_w \qquad (3)$$

Where,
I … current through the wire in the circuit
R_w … wire resistance at temperature T_w (wire temperature)
To find Q_T, the value of heat transferred to the fluid, it is necessary to relate the wire resistance and general heat transfer equations. The wire resistance as a function of temperature can be described by the following series of expressions:

$$R_w = R_o[1 + C(T_w - T_o) + C_1(T_w - T_0)^2 + \cdots] \qquad (4)$$

Where,
R_0 … wire resistance at a given initial reference temperature
T_0 … initial wire reference temperature
T_w … fluid temperature
C … temperature coefficient of resistivity
Disregarding the higher-order terms, and applying the boundary condition $R_o = R_g$ when $T_0 = T_g$ the following expression results:

$$\Delta T = \frac{\mathrm{R_w} - \mathrm{R_g}}{\mathrm{R_o C}} \qquad (5)$$

R_g … wire resistance when the wire temperature equals that of the fluid to be measured.
ΔT … temperature difference between the wire and the fluid $(T_w - T_g)$

The following is a good empirical equation for describing heat transfer for a fluid flowing over an infinite rod:

$$Nu = 0.42Pr^{0.2} + 0.57Pr^{0.33} + Re^{0.50} \qquad (6)$$

Where,
$Nu = \frac{hd}{k}$ (Nusselt number)

$Pr = \frac{\mu C_p}{k}$ (Prandtl number)

$Re = \frac{\rho U d}{\mu}$ (Reynolds number)

and where,

U … velocity of the flow
h … convective heat transfer coefficient
d … characteristic length (wire diameter in this case)
k … fluid thermal conductivity
μ … dynamic viscosity of the gas
ρ … gas density
C_p … specific heat of the gas at constant pressure

We may get the following formula for Q_T by ignoring radiation and conduction through the wire and assuming just convection:

$$Q_T = hA_s\Delta T \qquad (7)$$

Where,
A_s = Surface area of the wire exposed to the fluid flow
Substituting Equations (5) and (6) into (7), and adding some algebraic manipulation, the following expression results:

$$Q_T = (R_w - R_g)(X + Y\sqrt{U}) \qquad (8)$$

Where,

$$X = \frac{0.42kA_s}{R_0 Cd}\left(\frac{mC_p}{k}\right)^{0.2} \qquad (9)$$

m … the mass of the probe

And,

$$Y = \frac{0.57kA_s}{R_0 Cd}\left(\frac{mC_\rho}{k}\right)^{0.33}\left(\frac{rd}{m}\right)^{0.5} \qquad (10)$$

The following formula is obtained by substituting Equations (3) and (8) into Equation (2) and defining a resistance ratio as $R = R_w/R_g$:

$$I^2 = \left(\frac{R-1}{R}\right)(X + Y\sqrt{U}) \qquad (11)$$

For a given wire, the value of R is constant so that Equation (11) can be simplified to:

$$I^2 = A + B\sqrt{U} \qquad (12)$$

King's Law is the name given to this equation. The square root of related known velocities, $\sqrt{U}$, is plotted against the second power of the observed values for the current I^2 to calibrate the hot-wire anemometer. It can also be in a voltage format with different constants' units more will be later expressed.

A perfect match straight line may be fitted to the data, allowing the values of Equation (12)'s constants A and B to be calculated.

It's important to remember that analysis simplifies what's going on within the hot-wire anemometer. The axial heat conduction in the wire, heat loss at the wire attachment locations on the probe, aero-elastic behaviour of the wire, and the dynamic system response for both the heated wire and the measurement circuit would all need to be included in a comprehensive study.

Furthermore, while calibrating and using hotwire anemometers, several measurement errors must be taken into consideration. These include but are not limited to:

1- Calibration measurement errors - the errors in measuring the calibration flow parameters and hot wire voltages.
2- Calibration equation errors - the errors resulting from the fitting of a calibration equation, as well as the solution of the calibration equation and the lookup table.
3- Calibration drift errors - the errors imposed by probe contamination, as well as fluctuations in calibration over time and switching the feedback circuitry on and off.
4- Approximation errors - the errors resulting from assumptions made about the flow field when solving the calibration equations.
5- High-frequency errors - the errors induced by high-frequency changes in hot wire behaviour.
6- Spatial resolution errors - the errors induced by the flow field's spatial averaging.
7- Disturbance errors - the errors resulting from the probe obstructing the flow field.

The effects of natural convection also contribute to uncertainty in the calibration at low flows. The heated wire still transfers heat energy to the environment even when the velocity in the calibration wind tunnel is set to zero thanks to natural convection buoyancy effects [2].

1.3 PROBE MODES

There are two main modes of operation for hot-wire anemometry: the constant temperature mode and the constant current mode. The former keeps the wire temperature (T_w) at a constant value throughout the operation via means of an electrically managed feedback signal through a Wheatstone bridge circuit and the latter keeps the current at a steady value. This thesis focuses on the constant temperature operating mode [5].

In the constant temperature running mode, the resistance of the probe's sensor material changes with changing temperature of the surrounding fluid. The output electric signal from the hot-wire sensor additionally adjusts in accordance with each freestream velocity and freestream temperature variation since the wire component is sensitive to environmental temperature and flow velocity [5].

Therefore, it is crucial to convert the measured output voltage signal to a flow velocity with a proper temperature correction approach for quantitative velocimetry. In the case when the flow temperature variation for the duration of the experimental operation period (e.g., wind tunnel running duration) is negligibly small, the output voltage signal can be clearly considered as a function of solely the flow velocity. In this case, King's law is employed to convert the voltage signal to the flow velocity. Which is expressed as,

$$E^2 = a + bU^n; n \in [0.45\ , 0.5] \qquad (13)$$

Here, constants *a* and *b* are calculated by using a range of known flow velocities with a regular least squares suit for *a* and *b* [5]. This form of King's law is used in practice more often. We change to voltage format because the reading from the hot-wire is in Volts.

Meanwhile, in case the temperature fluctuation in the flow during the running operation is large, the temperature dependence can no longer be neglected and the measured voltage signal turns into a characteristic of both flow velocity and temperature. In this case, Hultmark et al. recommended a temperature correction approach, which is expressed as,

$$U = v \cdot f\left(\frac{E^2}{k\Delta T}\right) = v \cdot f\left(\frac{E^2}{k(T_w - T_a)}\right) \qquad (14)$$

where f denotes a functional dependence, v is the kinematic viscosity, and k is the thermal conductivity of air. Since both variables (v and k) are dependent on the freestream temperature T_a, v can be found by using Sutherland's law and air density, and k can be obtained from an empirical model. Note that this method was proposed for the subsonic flow regime. This technique is useful when only a single velocity calibration with a known ΔT is sufficient, but the wire temperature T_w must be known. A slight modification of the method is needed when the wire temperature is unknown [5].

Hot-wire anemometry is useful in measuring unsteady flow characteristics such as boundary layer turbulence via utilizing its quick response [5].

1.4 TECHNICAL BACKGROUND

Hot-wire anemometry is primarily based on convective heat transfer from a heated sensing element. The most frequent sensor configurations are cylindrical hot wires and hot films deposited on cylindrical fibres. The concept introduced – hot-wire anemometry – applies

mainly to these two kinds of sensors. However, different kinds of hot-film probes are also used, and the idea can be modified to include such sensor configurations. Many of the heat-transfer factors are similar for each hot-wire and hot-film probe, and the term hot-wire will cover each of these probe types, except otherwise stated. Features that belong particularly to either hot-wire sensors or hot-film sensors are recognized in the text.

The heat transfer from a heated wire positioned in a fluid flow relies upon both the properties of the ambient fluid (density, ρ, viscosity, μ, thermal conductivity, k, and particular heat, c_p, etc.) and the parameters of the flow (velocity vector, $\vec{U}$, fluid temperature, T_a, pressure, p, etc.).

1.4.1 FINITE LENGTH HOT-WIRE SENSORS

The heat transfer from a hot-wire probe containing a finite element ratio sensor (see figure (2)) deviates from that of an infinitely long wire [6]. The sensing element can also be prolonged until the prongs, as shown in figure (2),

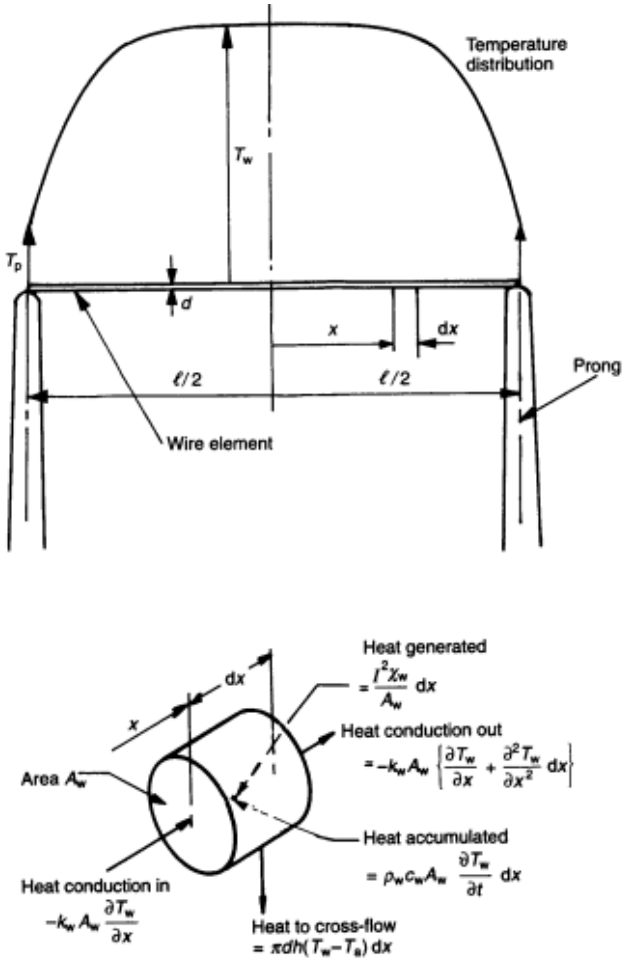

Figure 2. The hot-wire geometry and heat balance for an incremental element [6].

or the active part of the wire (the sensing part of the probe) can also be separated from the prongs through a plating technique while keeping the physical connection of the electrical wire. In contrast with the wire element, the prongs are massive, and the prong temperature, T_p, will consequently continue to be at a temperature close to the time-mean ambient fluid

temperature, $\bar{T}_a$. Since the wire is operated at an increased temperature, conductive heat transfer will take place in the direction of the prongs, ensuing in a temperature distribution within the wire element [6]. This temperature distribution can be determined from the heat-rate balance equation for an incremental wire element, *dx,* (see figure (2))

$$\mathrm{d}\dot{Q}_e = \mathrm{d}\dot{Q}_{\mathrm{fc}} + \mathrm{d}\dot{Q}_{\mathrm{c}} + \mathrm{d}\dot{Q}_{\mathrm{r}} + \mathrm{d}\dot{Q}_{\mathrm{s}} \qquad (15)$$

where $\mathrm{d}\dot{Q}_e$ is the electrical heat-generation rate, $\mathrm{d}\dot{Q}_{\mathrm{fc}}$ is the forced-convective heat-transfer rate, $\mathrm{d}\dot{Q}_{\mathrm{c}}$ is the conductive heat-transfer rate, $\mathrm{d}\dot{Q}_{\mathrm{r}}$ is the radiation heat-transfer rate, and $\mathrm{d}\dot{Q}_{\mathrm{s}}$ is the heat storage rate [6].
The individual terms in eqn (15) can be expressed as the heat-generation rate by an electrical current, I,

$$d\dot{Q}_e = \frac{I^2 \chi_w}{A_w} dx \quad (16)$$

the place χ_w, is the electrical resistivity of the wire material at the local wire temperature, T_w, and A_w, is the cross-sectional area of the wire. The forced-convection heat-transfer rate, $\mathrm{d}\dot{Q}_{\mathrm{fc}}$, to the fluid can be expressed in terms of the heat-transfer coefficient *h*, as

$$d\dot{Q}_{fc} = \pi dh(T_w - T_a)dx \quad (17)$$

Figure (2) shows that the total conduction heat-transfer rate out of the element is

$$d\dot{Q}_c = -k_w A_w \frac{\partial^2 T_w}{\partial x^2}\, dx \quad (18)$$

where k_{w} is the thermal conductivity of the wire material at the temperature T_{w}. The radiation heat-transfer rate is

$$d\dot{Q}_r = \pi d\sigma\varepsilon(T_w^4 - T_s^4)dx \quad (19)$$

where σ is the Stefan-Boltzmann constant, ε is the emissivity of the sensor, and T_s is the temperature of the surroundings. In most hot-wire anemometry applications this term is very small, and it is omitted. The heat-storage rate then is

$$d\dot{Q}_s = \rho_w c_w A_w \frac{\partial T_w}{\partial t}\, dx \quad (20)$$

where ρ_{w} is the density of the wire material and c_{w} is the specific heat of the wire material per unit mass [6].

By inserting these relationships in eqn (15) the following equation can be obtained

$$k_{\mathrm{w}} A_{\mathrm{w}} \frac{\partial^2 T_{\mathrm{w}}}{\partial x^2} + \frac{I^2 \chi_{\mathrm{w}}}{A_{\mathrm{w}}} - \pi dh(T_{\mathrm{w}} - T_{\mathrm{a}}) - \rho_{\mathrm{w}} c_{\mathrm{w}} A_{\mathrm{w}} \frac{\partial T_{\mathrm{w}}}{\partial t} = 0 \qquad (21)\ [6]$$

1.5 PROBE DESIGN AND MANUFACTURING

Hot-wire anemometry structures typically consist of a probe to support the sensor filament, electrical wires, and the anemometer electronics that manipulate the sensor heating current [1].

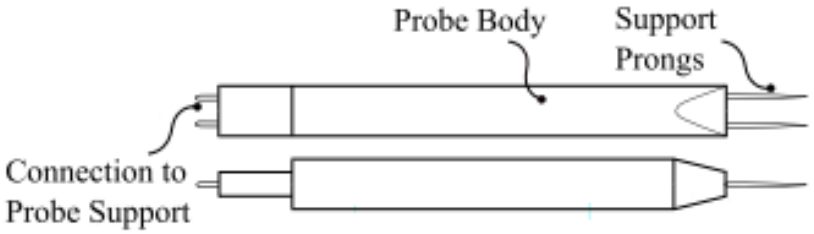

Figure 3. Schematic of a typical hot-wire probe [1].

Figure (3) shows a schematic of a standard hot-wire probe [7]. The sensor filament (not shown) attaches to the cease of the two support prongs, which are linked to the probe body. The probe body presents a secure, low-vibration mechanical support, and additionally contains the electrical wires from the prongs to the base connectors. It is frequent to design, and construct hot-wire probes in order to meet particular environmental requirements [3]. For example,

1.5.1 WESTPHAL ET AL

Westphal et al developed more than one hot-wire probe design with platinum sensor wire. They proposed an active sensing length of 200μm to collect correct measurements of Reynolds stresses very close to solid surfaces. A sensor fabrication process was developed, the usage of an acid jet to etch the silver coating of Wollaston platinum wires barring any additional re-plating, to manipulate the sensing length of the wire [8].

1.5.2 YASA ET AL

Yasa et al developed a hot-wire probe that carried two hot-wire sensors and one thermocouple, placed between the two hot-wire heads. This allowed for simultaneous temperature to correct temperature editions in the flow [9].

1.5.3 INASAWA ET AL

Inasawa et al developed a hot-wire probe with a small constant temperature anemometry (CTA) gadget and a short sensor cable. The CTA circuit board was once enclosed in a metallic container installed immediately on the hot-wire support stem. This allowed for the immersion of the complete gadget in the flow, to enhance the signal-to-noise ratio in the CTA measurements [10].

1.5.4 SUBRAMANIYAM ET AL

Subramaniyam et al used a DISA 55A75 slanted high temperature hot-wire probe inner an internal combustion engine cylinder, pushed through an electric powered motor. The maximum cylinder temperature was stated as 674 K, due to compression. The implied velocity was much less than 14 m/s at all measurement locations. The low flow pace considerably reduced the feasible complications of the experiments. The wires were calibrated

at room temperature without using any temperature compensation techniques to take account of the difference between the calibration temperature and the temperature all through their experiments. Uncertainty evaluation was now not provided in this work to quantify the measurement error due to temperature variations [11].

The prementioned hot-wire probe designs have been shown to be incredibly advantageous for typical, reasonable temperature, low-velocity flow conditions. The elements of these probes are no longer designed for high-temperature flows. While industrial high-temperature probes can face up to these temperatures, their sensor wires are extraordinarily susceptible to separation from the prongs at excessive velocities. These problems encouraged the design of a custom, high-temperature probe, and to enhance a sensor attachment method to acquire a sturdy anemometry system for high-temperature, high-velocity flows [3].

1.6 CALIBRATION METHODS OF HOT WIRE ANEMOMETRY

This kind of measurement (hot wire anemometry) is indirect, having a voltage signal as its output. As a result, the need for calibration is vital for effective and precise velocity measurement. The calibration of a hot-wire anemometer for high velocities (about $U \geq 1.5$ m/s, where U is the calibration velocity) may be done simply with a pitot-static tube and a manometer using conventional ways. However, because the pressure differential (dynamic pressure) inflow is so small that it is difficult to read precisely with a manometer, the calibration of a hot wire anemometer for low velocities (particularly $U < 1.5$ m/s) cannot be done using this traditional calibration approach [13].

Many scientists have devised alternative ways for low-velocity calibration of hot-wire anemometers. The laminar pipe-flow approach, the calibration method based on a moving hot-wire anemometer with a known velocity in a stagnant medium, and the shedding-frequency method is the most often used. There are other calibration jets and low-velocity calibrators on the market. The TSI 1125 calibrator, for example, may be utilized for low-velocity ranges of 0.02 m/s to 0.9 m/s. The pressure drop from the calibration jet's plenum chamber is monitored and utilized to calculate velocity from the given graphs in this calibration jet [12].

1.6.1 KOHAN AND SCHWARZ

Kohan and Schwarz [14] used the shedding-frequency method and calibrated a hot-wire anemometer at low velocitys using Roshko's [15] Strouhal–Reynolds number (SR) relationship for flow Reynolds numbers ranged between 50 and 150. The velocity was calculated using the SR relationship after measuring the vortex-shedding frequency.

Periodic vortices are shed from a circular cylinder in a uniform velocity field above a cylinder with Reynolds number Re above 40, where U and d are the free-stream velocity and cylinder diameter, respectively. On plots of S vs Re (for example, see Roshko [15]), data covering a wide range of free-stream velocities and cylinder diameters correlate well if the shedding frequency f from one side of the cylinder is described in terms of the Strouhal number S, where $S = f \cdot d\ /U$. However, because U exists in both dimensionless groups, the velocity cannot be determined from these curves when the shedding frequency f is recorded. A dimensionless number Ro containing the frequency, but not the velocity, is given by

$$R_o = S \cdot Re = \frac{f \cdot d^2}{\nu} \qquad (22)$$

Roshko appears to be the first to show how useful this number is. In terms of experimental consistency, the region of regular vortex shedding, $40 < Re < 150$, is most suitable for calibrating purposes [16]. Tritton [24], based on his discovery of a secondary transition around $Re \doteq 90$, offered a revision of Roshko's original equation for this area (Gerrard [25] pointed out that the additional break in the curve for this Reynolds number range discovered by Tritton may reflect the change between two- and three-dimensional vortex shedding from the cylinder). Dubiously, Webster [26] discovered that Roshko's empirical equation for Ro versus Re in the range $Re > 300$ (turbulent vortex shedding) yielded constant results in Webster's tunnel spanning the range $50 < Re < 590$, but Tritton's formulas did not. The background turbulence level is different from one another for Webster and Roshko (Roshko, 0.03%; Tritton, unreported; Webster, about 3%). Although Collis and Williams [27] report no measurable effect of background turbulence level on shedding frequency in the region $Re < 90$, this effect has not been fully investigated and remains a possible explanation for Webster's results [14].

1.6.2 CHRISTMAN AND PODZIMEK

Christman and Podzimek [16] used the nozzle of a DISA 55D41/42 calibrator to calibrate a hot wire.

The forced velocity exerted on the hot-wire probe is created by slowly draining water from an airtight tank attached to the calibration nozzle where the probe is placed. Figure (4) illustrates a schematic layout of the relative positions.

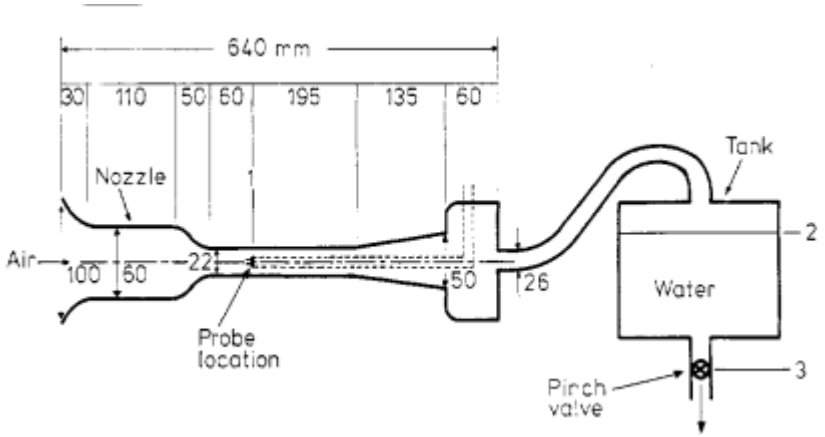

Figure 4. Schematic of the equipment the nozzle is part of a set of DISA 55D41/42 calibrating equipment that may be employed horizontally or vertically. The DISA 55Pll straight-wire probe has a 30 mm stem length and a 2 mm stem diameter. It has 5 mm long prongs [16].

The probe's first location is within the calibration nozzle. The water surface within the tank is located at position 2, and the water discharge control is located at position 3. In the following discussion, these location numbers will be utilized as subscripts whenever applicable.

As water drops from 3, the water level 2, falls from $y = A$ to $h = B$ in time $t = \tau$. The rate at which water exists at 3 is calculated using Bernoulli's equation. Assuming constant water density and using position 3 as a reference level, one may calculate the velocity at the point 3 in the simple form $U_3 = \sqrt{2gy}$ if the cross-section $a_3 \ll a_2$. (In this case $a_3 = a_2/278$.) Continuity allows the velocity at 2 to be expressed in terms of U_3 as

$$U_2 = Dy^{0.5},\ D = Pa_3(2g)^{0.5}/a_2 \qquad (23)$$

The constant D has been developed as the coefficient of discharge, P, to allow for friction. The velocity at 2 may also be expressed by

$$U_2 = -dy/dt = -D^2t/2 + DA^{0.5} \qquad (24)$$

It is important to establish an equation for D in terms of observed values in order to determine D empirically. This may be done by calculating the average value of U_2 between A and B, as shown in (24):

$$\tau^{-1}\int_A^B -dy = \tau^{-1}\int_0^\tau [-D^2t/2 + D(A)^{0.5}]dt \qquad (25)$$

which results in the expression

$$D_{1,2} = 2[(A)^{0.5} \pm (B)^{0.5}]/\tau \qquad (26)$$

When compared to real data, the correct root is

$$D = D_2 = 2[(A)^{0.5} - (B)^{0.5}]/\tau \qquad (27)$$

Consequently, (24) now becomes

$$U_2 = 2[(A)^{0.5} - (B)^{0.5}](h)^{0.5}/\tau \qquad (28)$$

For all velocities less than $200\ \text{mm s}^{-1}$, the flow at 1 (250 mm from the tube entrance) is laminar and exhibits a parabolic velocity profile. As a result, the hot-wire probe's actual velocity, *U*, is double the average (or volumetric) flow velocity, implying that

$$U = 2U_1 = 2(d_2/d_1)^2U_2 \qquad (29)$$

The air velocity at the probe is now a function of the time, τ, it takes for the water tank to drain from point *A* to point *B*, and of h at the measurement point. Measurements were taken at *h*, the mean value of *A* and *B*, for the purpose of simplicity it is used,

$$U = \frac{K}{\tau},\ K = 4(d_2/d_1)^2[(A)^{0.5} - (B)^{0.5}](y)^{0.5} \qquad (30)$$

Filling the tank to *A* and then letting it empty at a rate controlled by the pinch valve were used to make the measurements. The bridge voltage, V_B, was read from the DVM and recorded as the water level surpassed h. The time was recorded, and the timer was reset at the conclusion of each run. As a result, V_B was closely tied to u, a time function, as illustrated by (30). The accuracy of (30) was determined by calculating the maximum degree of inaccuracy achievable in each direction from the zero-error value. All distances measured were thought to be correct to within 0.5 mm, and time was thought to be accurate to within 0.05 s. The lowest values of A and B (i.e., the heights of the shortest tank probes) were used, together with a fictive time, τ, equating roughly to 10 mm/s, to maximize the effect of measurement error. The observed *U* = 10 mm/s might be wrong by as much as + 22 % or – 18 % in the very rare scenario that all of the measurements were off by their respective maximum percentages [16].

1.6.3 BRUUN ET AL.

A swing-arm setup was used by Bruun et al. [19] to calibrate hot-wire at low velocities.The suggested approach may be used to create either a linear or circular motion theoretically. A swinging arm test facility was utilized to establish the method's viability, with the probe at the end of a vertical swinging arm in a gravitational field.

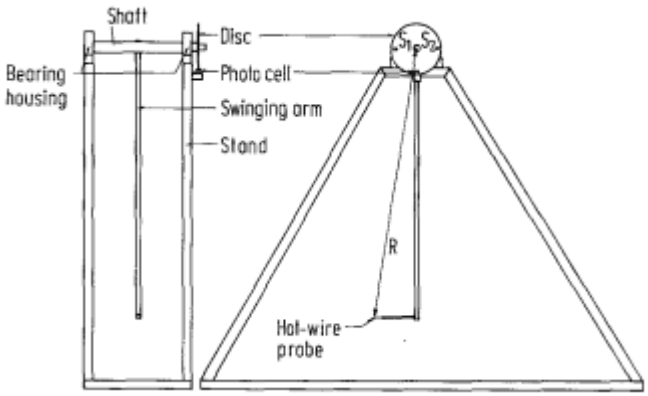

Figure 5. Front and side view of swinging arm test rig [19].

Figure (5) depicts the swinging arm testing setup. The test rig consists of a swinging arm attached to a rotating shaft positioned on a pedestal, as can be seen. High-quality cylindrical roller bearings were installed at either end of the shaft to decrease friction in the system and consequently vibrations that may taint the anemometer data. The shaft was also hollow on one side to allow cable connection from the probe to the anemometer set. The approach is based on the application of a constant length S of the probe path and its identification. As illustrated in figure (6), this goal was achieved by inserting a disk on one end of the spinning shaft. Two machined slots at the perimeter of this disk were spaced at an angle of $\Delta\theta$. This disk (and the slots) is driven by a slotted photocell unit with an integrated infrared source and a photo detector. As slit S1 passes through the photocell, it initiates digital sampling of the output from the hot-wire anemometer, which will continue until the second slit S2 passes through the photocell, stopping the acquisition of new data. Because the arm swings like a pendulum, the slits revolve past the photocell again, the photocell was configured to only switch sampling on and off once.

Table 1. Calibration constant, for three separate tests [19].

Test	**A**	**B**	**C**
A	1.3087	0.9408	0.4399
B	1.3124	0.9432	0.4363
C	1.3112	0.9445	0.4365

Table (1) shows the results of the three tests A, B, and C. Two assessments will be provided to demonstrate the differences between the three curve fits corresponding to tests A, B, and C. Initially, setting $U = 1\ \mathrm{m/s}$ and $6\ \mathrm{m/s}$ it was evaluated that the variation between the corresponding calculated voltages for the three methods is

$$1\ m/s: \quad E = 1.5013\ V \pm 0.0013\ V$$
$$6\ m/s: \quad E = 1.8374\ V \pm 0.0007\ V$$

In other words, the observed voltage uncertainty is around 1 mV. By assuming that one of the tests (e.g. test A) represents the right response, the related velocity uncertainty may be calculated. This allows the assessment of the associated voltage value E for each specified velocity *U*, which can then be utilized as an input to test B and C to determine the corresponding velocities.

Table 2 Comparative velocity evaluation using test A as a reference [19].

$U_A\ (m/s)$	$U_B\ (m/s)$	$U_C\ (m/s)$
1	0.985	0.985
3	2.993	2.987
6	6.029	6.014

Table (2) shows a comparison for U_A = 1, 3 and 6 m/s, with the largest change being 0.03 m/s (0.5 % at 6 m/s). This precision outperforms both "sled" motion and dynamic calibration [19].

1.6.4 LEE AND BUDWIG

In the low-velocity range between 0.15 m/s and 0.95 m/s, Lee and Budwig [12] developed two methods: the laminar pipe-flow method and the shedding-frequency method.

The laminar pipe-flow method: A modified TSI 1125 calibrator was utilized for the low-velocity hot-wire calibration. The setup for getting low-velocity measurements is shown in figure (6). To guarantee steady temperature and equal flow at the entry of the glass calibration tube, the calibration equipment included a heat exchanger and the plenum chamber/ contraction of a TSI 1125 calibrator. A specifically made adapter was used to attach a glass tube at the outlet of the contraction of a TSI 1125 calibrator. The glass tube had a diameter of 2 cm and a length of 80 cm. The glass tube's length was designed to allow fully developed laminar pipe flow at the tube's exit plane.

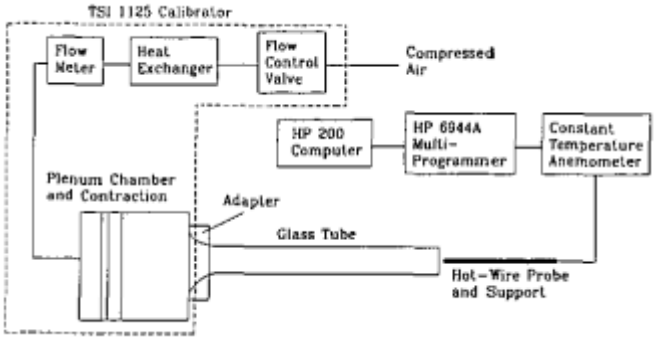

Figure 6. Pipe flow apparatus for the calibration of hot-wire anemometer at low wind velocities. The glass tube and hot-wire probe were oriented vertically in the laboratory [12].

The shedding-frequency method: The shedding frequency is determined in this approach, and the velocity is calculated using an empirical SR relationship. Unfortunately, published SR curves for low-velocity calibration in the relevant Reynolds number range exhibit variances of up to 20%. An accurate calibration method based on cylinder vortex shedding was developed using flow visualization and hot-wire anemometry. Smoke-wire flow visualization was used to analyze the vortex-shedding modes of a circular cylinder, and hot-wire anemometry was used to produce the associated SR curves [12].

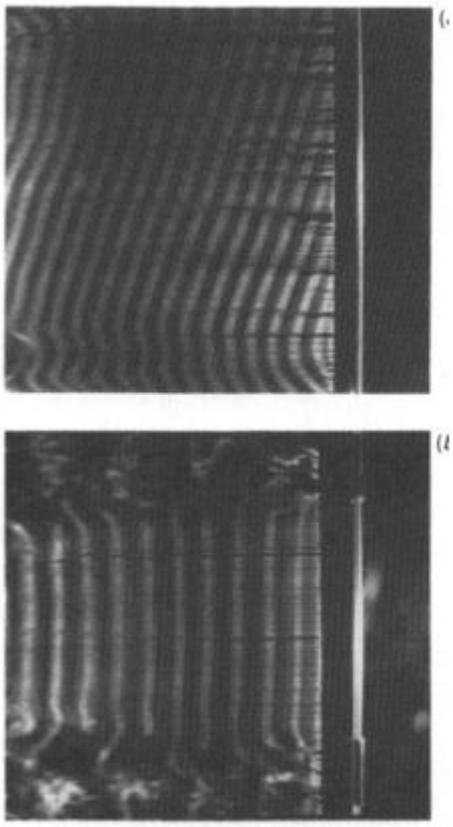

Figure 7 Spanwise flow visualization of the vortex street wake a circular cylinder, R=130 for both; (a) oblique vortex shedding mode for a cylinder with no end modification; (b) parallel shedding mode due to end cylinders [12].

Figure (7) compares the calibration findings from three different methods: (i) the pipe-flow method, (ii) shedding-frequency, and (iii) the TSI I125 calibrator. Figure (8) shows that the laminar pipe-flow approach (open circles) determines free-stream velocities that are within ±3% of those reported by the shedding-frequency method (full line). The pipe-flow calibration findings have a ±1.5 cm/s margin of error. Figure (8) further demonstrates that the TSI 1125 calibrator's free-stream velocity (open rhombuses) was 4-50 percent lower than the calibration findings of the current techniques [12].

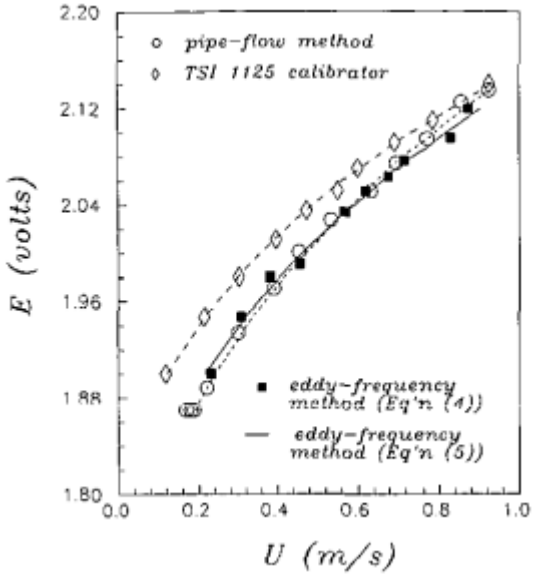

Figure 8. Calibration results of the two improved methods and the TSI 1125 calibrator in the low-velocity range [12].

1.6.5 YUE AND MALMSTRÖM

In the low-velocity range of 0.1 m/s and above, Yue and Malmström employed a laminar pipe-flow approach for a hot-wire anemometer.

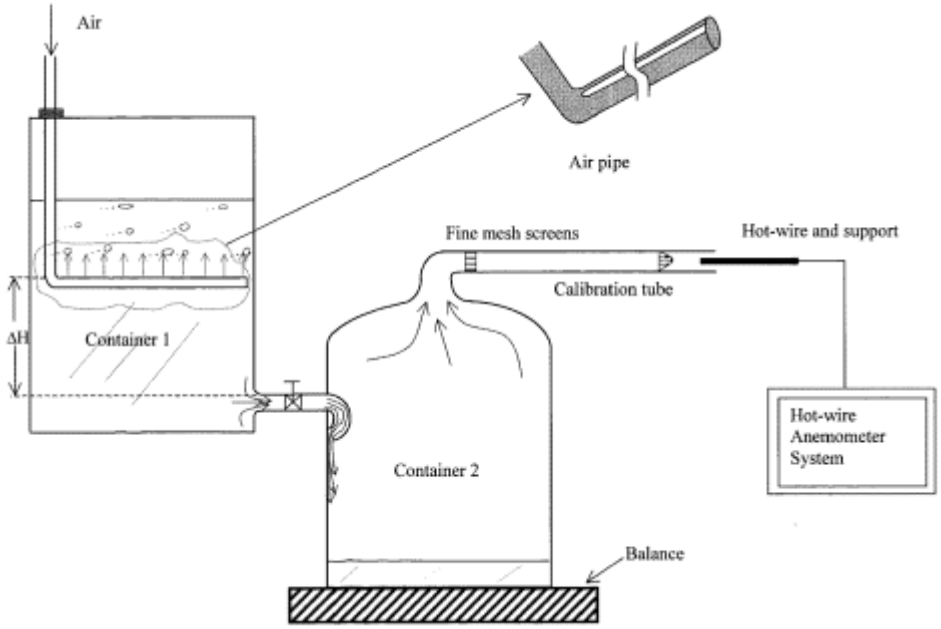

Figure 9. A sketch of the apparatus for the calibration of hot-wire anemometers at low velocities [21].

Figure (9) illustrates the entire calibration setup. It is made up of two airtight containers, one of which contains an adjustable pipe, as well as some flexible plastic connecting pipes and a copper calibration pipe. The first container's purpose is to keep the water flowing into the second container at a steady rate. Because the pressure at the level of the horizontal section of the air pipe will be constant as long as the water level in container 1 is above the opening slit of the air pipe, this is possible. A particularly constructed air pipe, which is a copper pipe bent at 90° angles and shaped like a half square, provides a constant flow. The air pipe's upper end is exposed to the outer atmosphere. The bottom portion of this pipe runs parallel to the container's bottom surface. At the top of the horizontal section of the pipe is a long slit. The slit is approximately 1.5 mm wide.

Table 3. Measurement of uncertainties of instruments [21].

	Instruments	Measurement range	Uncertainties
Weight	Sartorius IC64	0–64 kg	±1 g
Time	Seiko Plastic		±0.2 s
Temperature	Testo 610	−5 to 50 °C	±0.2 °C
Relative humidity	Testo 610	10–96%	±1.5%

All the equipment used in this study has SP calibration certificates (Swedish National Testing and Research Institute), and the uncertainties of these instruments are listed in table (3). The equipment utilized for the calibrations have an overall l uncertainty of less than 1.5% [21].

1.6.6 AL-GARNI

Al-Garni [23] used a calibration system based on moving hot-wire probes in stagnant air to calibrate a hot-wire anemometer in the low-velocity range of 0–0.15 m/s.

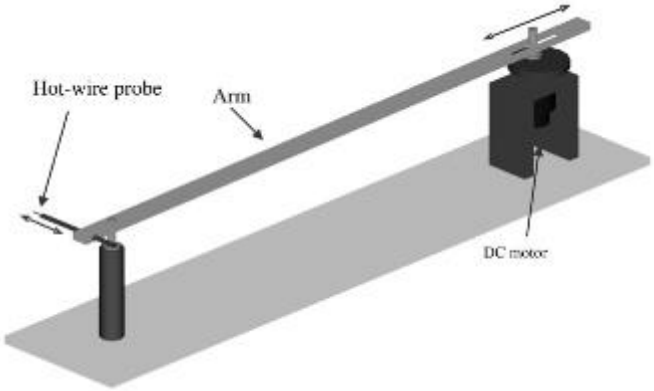

Figure 10. 3D view of the calibration device [23].

Figure (10) illustrates a device for calibrating hot-wire anemometers at low velocities. The calibrating method uses a hot-wire probe that is moved in stagnant air. Therefore, the following conditions must be met: (i) the probe's velocity and corresponding anemometer signal must be precisely monitored, (ii) the fluid must be stagnant, and (iii) the probe's motion must be virtually free of vibrations [23].

At low velocities ranging from 0 to 15 cm/s, a calibration of the hot-wire probe was carried out. The DAQ was programmed to take 100.000 measurements at 1000 Hz. A dc offset of the hot wire signal was conducted to increase measurement precision, resulting in a hot-wire output resolution of about 0.586 mV. Furthermore, based on a 95 percent confidence level, the highest uncertainty in the measurements collected was around 4.1% [23].

1.7 VARIABILITY AND UNCERTAINTY

We will focus the discussion mainly on the observed variability, which is caused by two sources. The first is the variability in the measured signal, second is the variability in the measurement system. Since we can't affect this kind of variability, we will not discuss it so much. Main sources of variability in the measurement system can include [28]:

1- The operator
2- The method
3- Measured value
4- The measuring gauge
5- The environment

1.7.1 UNCERTAINTY MEASUREMENT

In the previous section, we discussed what would cause the uncertainty, but the important question now is how to estimate it?

It’s not easy to decide what is or where is the variability and find out its source. So, it’s suggested [28] to follow this tracing scheme:

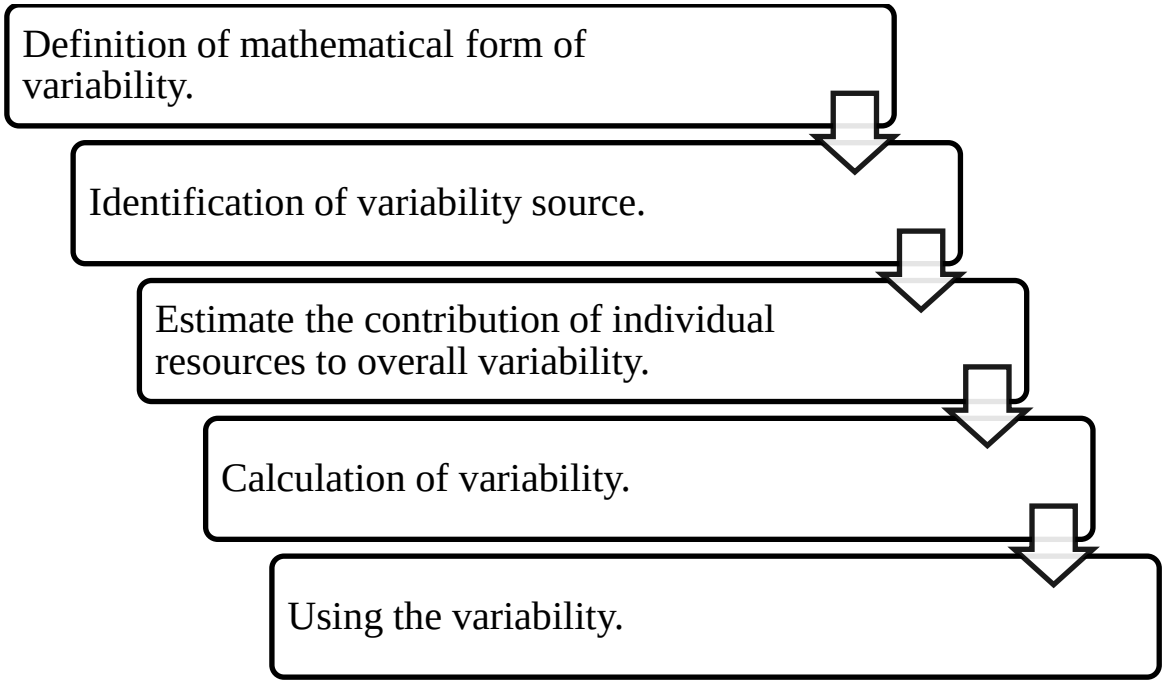

Figure 11. Scheme of numerical determination of variability [28]

1.7.2 SOURCES OF UNCERTAINTY

All sources of uncertainty can be divided into 2 main categories:

- Source type A
- Source type B

Type A sources are the sources that can be described only based on their total effect with the help of repeated measurements. It's determined by the means of statistics.[28].

On the other hand, type B sources (sources determined by the type B method) whose standard uncertainty:

- Cannot be determined by the type A method.
- Can be identified (searched by qualified analysis)

1.7.3 UNCERTAINTY MEASUREMENT WITH TYPE A METHOD

It's possible to use the A method only when it's possible to perform the measurement repeatedly [28].

Standard type A uncertainty u_A is given by the relation:

$$u_A = \frac{s}{\sqrt{n}} \quad (31)$$

Where: s … standard deviation from repeated measured values,

n … number of iterations of the measurement,

The relationship (31) is from a statical point of view, the standard deviation of the arithmetic average. It's obvious that the smaller the u_A

- the deviation of the repeated measured values is smaller,
- the number of iterations will be bigger (if the s doesn't change) [28].

In case the measurement is repeated less than 10 times, then it's recommended to multiply the uncertainty u_A with a proper coefficient as given in [28].

1.7.4 UNCERTAINTY MEASUREMENT WITH TYPE B METHOD

In addition to the influences described by the type A method, the measurement system is affected by sources that can be identified in terms of the specific cause, the magnitude of variability, and statical behaviour without the need for repeated measurements. Another important feature of these types of uncertainty sources is that:

- they're measured with nonstatistical methods,
- their influence cannot be reduced by repeated measurements.

Type B uncertainties can be calculated in three ways:

1- from the already known expanded uncertainty by conversion to combined uncertainty,
2- by estimation from source variability and statistical distribution,
3- from a known combined uncertainty data from certificates and literature sources [28].

1.8 DIFFERENT MEASUREMENT METHODS

	Pitot static measurement	**Hot wire anemometer**	**Laser Doppler anemometer**
Principle	The velocity of the flow turns to pressure in the open of the pitot tube this is called the flow pressure, together with the static pressure reading can give the flow velocity. [29]	The fluid flow causes the current in the hot wire to alternate, the difference in the current is then translated to a flow velocity. [2]	Crossed laser beams hit particles in the flow, and the reflection of light is captured and transferred into velocity measurement. [30]
Equation	$U = C\sqrt{(2g(P_1 - P_2))}$ [29]	$I^2 = A + B\sqrt{U}$ [2]	$U = \frac{\lambda}{2 \cdot sin\left(\frac{\theta}{2}\right)} f_d$ [30]
Areas of use	Airplanes, wind tunnels.	Automotive (intake manifold), medicine, HVAC systems.	Experimental purposes, high accuracy flow measurements.
Advantages	Cheap, easy to use, small, no moving parts, low-pressure loss	Easy to set up, can be used in variable applications	No interruption for the flow, linear output signal. No wear for the measuring device.
Disadvantages	Interference with a physical process, low accuracy, needs high-velocity flows. [29]	Interference with a physical process, non-linear output signal. Wear and damage can occur with the filament or the wire. [2]	The necessity to use particles. A large instrument, practical for specific uses. [30]

2 METHODOLOGY

2.1 CALIBRATION WITH THE DANTEC CALIBRATOR

The hot wire system consists of various parts and devices that need to be connected with each other before attempting any measuring. For the wiring order, the probe is to be assembled to the base, which then must be connected to the multichannel CTA, from the multichannel CTA it should be connected to an A/D converter. The A/D converter main function is to read analogue signal from the CTA and translate it to a digital signal. The A/D signal must be connected to a computer or any proper device that will be able to read the digital signal and process it to the desired output. Power supply should be assured. To provide more accurate readings, usually a thermal sensor is connected to the system as well, but it's not essential. Figure (12) illustrates the connection of the hot-wire with the computer.

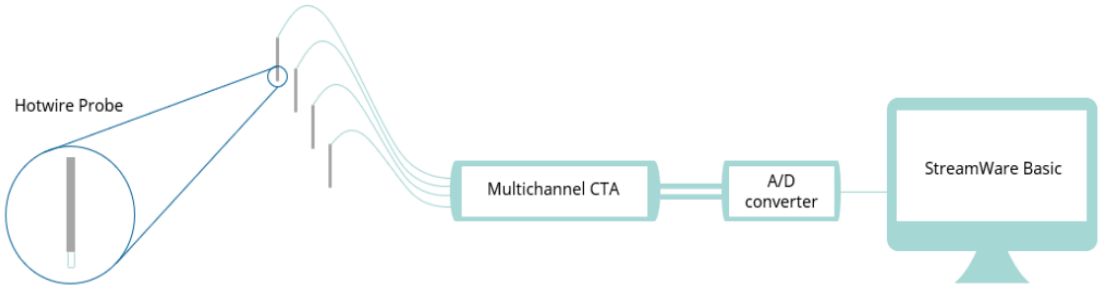

Figure 12. Multichannel CTA system [31].

It is crucial that the wiring matches the set, when the set is structured in the DANTEC software. Also, it is important to adjust the probe overheat in the software. To check that all the wiring and the set is well connected, multichannel case and A/D converter will light the ready LED. It is recommended that the wires are labelled to insure correct connection.

As for the first part of this experiment a DANTEC calibrator was used. The calibrator should also be connected to the multichannel case and to the A/D convertor since it is automatically controlled from the computer (the user). A high-pressure inlet gas should also be connected to the calibrator. The pressure that was used in this experiment with the calibrator was about 4 MPa. For this purpose, a compressor is needed to achieve such pressure. The gas that was used is air. The piping was with PVC fibre strengthen hose and quick connectors. The calibrator has changeable nozzles. For the purposes of low velocities in this experiment we used the smallest available nozzle. In order to hold the probe, a holder is needed to support the set.

After following the previous steps to start the calibration process using the DANTEC calibrator, the software was opened, choose the set, click on the calibration, set the type of calibration, in our case logarithmic, the number of points, the interval and the number of iterations to achieve each desired point, press start. For this experiment we choose 15 points from 0.02 m/s until 0.5 m/s.

Components of the experimental setup

1- Probe 55R01 (Figure 14)
2- Probe support 55H21
3- Probe holder
4- StreamLine pro automatic calibrator 9091H0013 (Figure 15)
5- Nozzle type 0, 1.4 mm^2
6- StreamLine multichannel frame 90N10 (Figure 13)
7- A/D convertor NI 9215 (Figure 16)
8- Cable A1863, 4 m
9- PC with Streamware Pro program from Dantec.
10- Airflow source
11- Piping connection
12- Compressor
13- Airflow valve

Figure 13. DANTEC multichannel Streamline frame 90N10

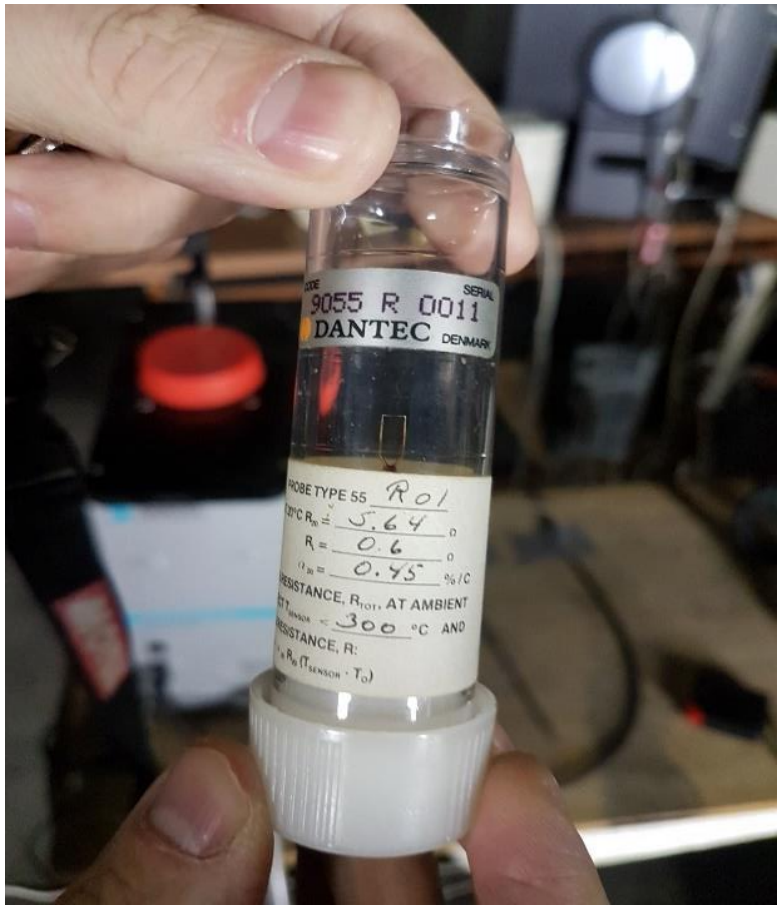

Figure 14. 1D Probe 55R01

Figure 15. DANTEC StreamLine pro automatic calibrator

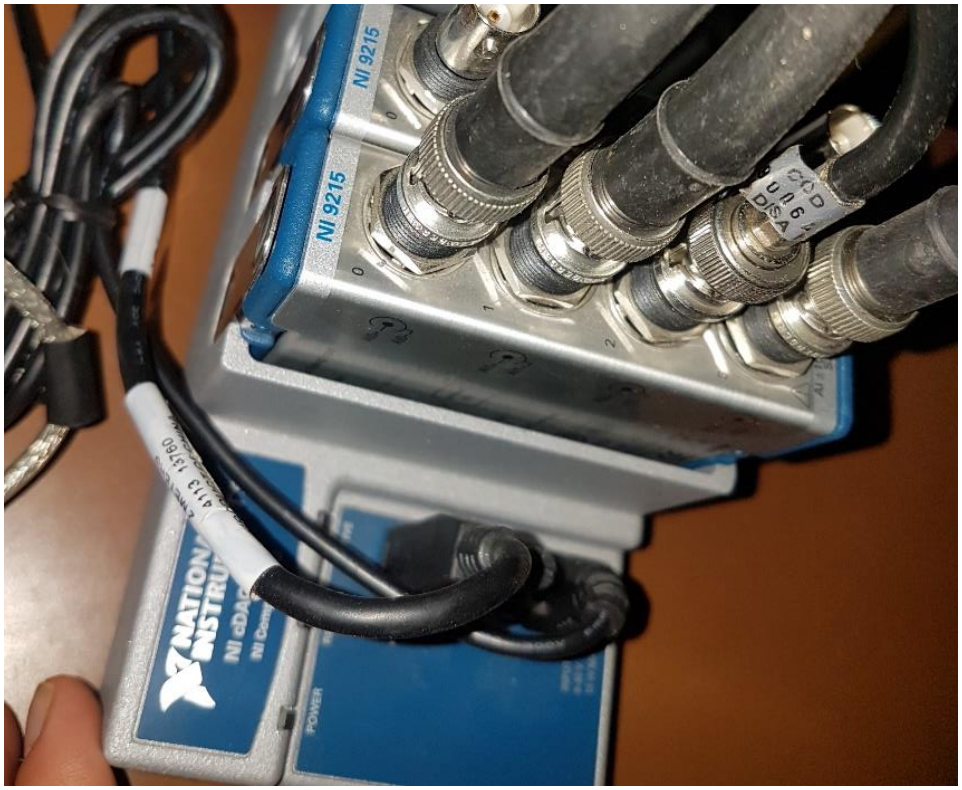

Figure 16. A/D converter NI 9215

2.2 CALIBRATION WITH THE NEW DESIGNED CALIBRATOR

Since this thesis is focused on low-velocity measurement, and it was intended to offer a simple and reliable alternative for the calibrator from DANTEC, that encouraged the new design. A diffuser was a necessity in the design since we needed to achieve low velocities. The diffuser needed to be 3D printed since it has specific dimensions. The output of the tube needed to be at least 10 times bigger than the hotwire dimension, to reduce the effect of heating the inner walls of the tube by the hotwire. The length was chosen to be long enough to ensure the developed flow. The inlet of the diffuser is also a known dimension. Knowing the inlet and the outlet of the diffuser, together with fluid mechanics tables helped us find the angle of the diffuser, respectively the length of it. The tube is a 50 cm long with an outer diameter of 110 mm (inner diameter 106 mm) from Marley. The calibrator was given the name HWC 1M. In order to achieve a relatively uniform laminar smooth profile, we needed to add flow straighteners to the design, a honeycomb and foam filter were used to fulfil that need. Figure (17) illustrates the design of the calibrator. In figure (18) is a simple illustration for the set together with the calibrator.

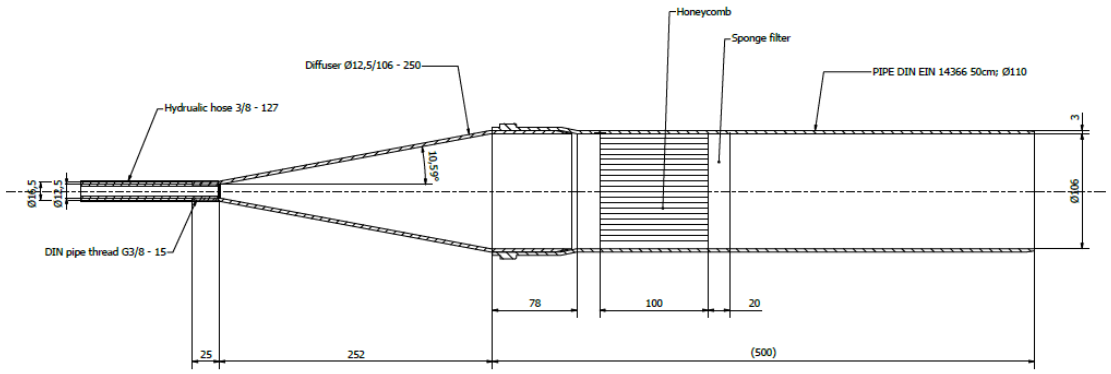

Figure 17. HWC 1M drawing

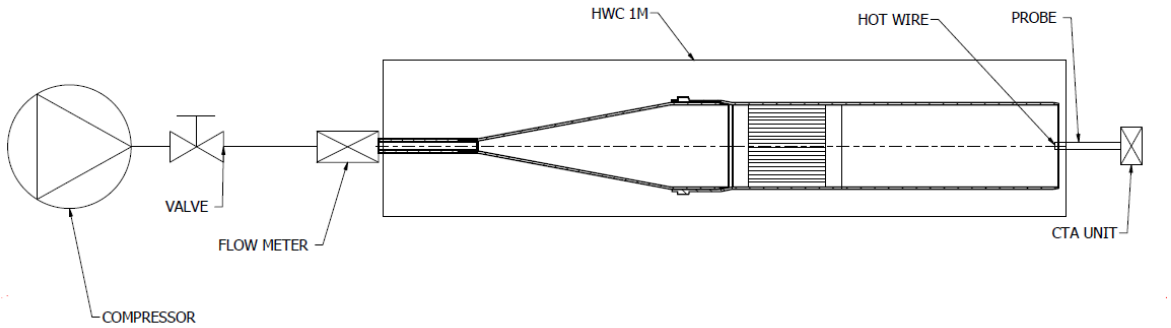

Figure 18. The set of the HWC 1M

The inner surface of the diffuser should be polished before assembling since the 3D printer prints it with rough surface (more about losses follows). The connection between the diffuser and the tube should be sealed to prevent any leakage which can result in some errors in calibration which will result in errors in the measurement respectively. The calibrator needs a flowmeter to measure the inlet flow. For that purpose, a TSI 5200 flowmeter was used, figure (19). The flowmeter gives the actual flowrate, the temperature of the fluid and the pressure of the flowing fluid. Note that when connecting the flowmeter, it's important to connect it as the arrow on it is showing the flow direction. The connection

is recommended to be guarded with clips to prevent leakage. It’s recommended to make the connection after the outlet of the flowmeter as short as possible to reduce the losses. Holders were used to hold the calibrator and the probe in place. Figure (20) illustrates the set after assembling. The flow was also provided from a compressor in the lab. The connection of the hot-wire set is the same as mentioned before. The flowrate, temperature and pressure reading were taken from the flowmeter and manually inserted to the software in a new added point in the manual calibration then the hot-wire provided the reading of the voltage for the corresponding flowrate. Then the point was updated, and the process was repeated to get enough points for the calibration. It’s recommended to get at least 10 points for the calibration. Then it is necessary to measure the velocity profile for a specific flowrate to get the profile coefficient for the velocity, to do so the flowrate was fixed, and the probe was set for different elevations through the diameter of the pipe. The profile coefficient depends on the flowrate so it’s necessary to measure multiple factors for different flowrates, and then interpolate the relation between the factors and flowrates. The equation from the interpolated curve then should be used to correct the readings. The readings were taken by changing the flow and taking the data from the CTA software.

Figure 19. TSI 5200

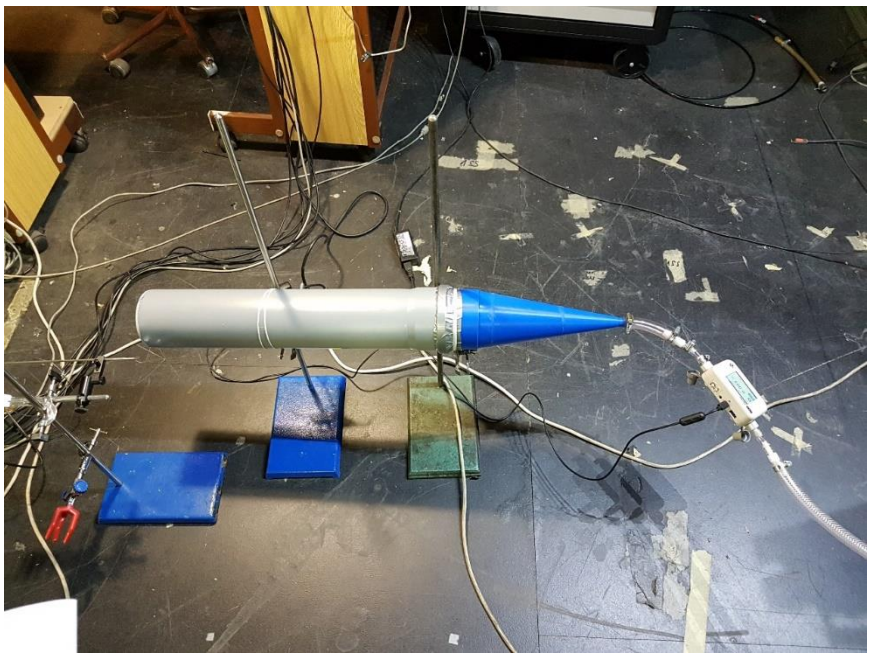

Figure 20. HWC 1M assembled

For the simplicity purposes some loses were neglected but for more accurate measurement they should be included. Minor factors that were neglected and can be evaluated for accurate readings are the diffuser pressure loss, the honeycomb (geometric loss), and the sponge filter (geometric loss), the length of the pipe (surface roughness loss), and the fittings losses (geometric loss). For each of these losses, we tried to minimize them as much as possible.

2.3 LASER DOPPLER ANEMOMETRY AS A REFERENCE

The measurement with the new designed model, have to be compared to a reference measurement. In this field (the fluid flowmeters) the laser Doppler anemometer is the most verified and reliable method usually used to calibrate other flowmeters. The Laser Doppler Anemometer, later will be referred to as LDA, uses the principle of light sensing method, it uses laser as a source of light. Different laser intensity changes the sensitivity to the device, and so for lower flowrates a more intense laser is needed to get accurate reading. Material is also needed for the sensor that receives the laser to capture its motion. For that purpose, smoke is pumped in the flow to insure the reflection of laser to the sensor (special camera). Note that the device can measure the velocity of the particles as well as their concentration. The more the data that is calculated for a reading, the more reliable that reading is. The data of one reading is then plotted in a gaussian distribution and from it gives the reading. Figure (21) illustrates the source of the laser and the laser dispenser of the LDA.

Figure 21. Laser source of the LDA

Figure (22) shows the set of the new calibrator in the LDA lab. The dark board in front of the laser helps to set the elevation of the laser beam to be in the centre of the tube (where the velocity is said to be maximum). The laser sensor must be aligned with a certain angel, in this experiment the alignment and the set of the LDA was done by the lab coordinator, Ing. Ondřej Cejpek (PhD student at the institute of energy in the faculty of mechanical engineering in Brno university of technology). Smoke was introduced at the outlet since it failed to distribute in the flow from the inlet side, due to the low velocity of the flow and it seemed that the honeycomb and the filter filtered most of particles introduced in the flow. The designed calibrator was connected to the flow together with the TSI 5200 flowmeter. The same issue of fluctuations appeared in the flow in this lab as well, so a flow controller is highly recommended for more accuracy. For each flowrate the smoke was introduced, the reading was taken on the software, the operation was repeated to cover the interval of the desired flow. The data of pressure and temperature were taken from the flowmeter.

Figure 22. Laser bisection lens and laser reader set with the HWC 1M

3 RESULTS AND DISCUSSION

3.1 MEASUREMENT WITH DANTEC CALIBRATOR

Several attempts for calibration were done before the best calibration results were chosen. The best results were chosen upon the calibration curve that they make, the closer it's to a logarithmic curve. The calibration as mentioned before is an automatic process using DANTEC calibrator.

Table 4. Calibration data using DANTEC calibrator 15.03.2022

U [m/s]	E1 [V]	T [C]	P [kPa]	E1corr [V]	U1calc [m/s]
0.020	1.400	16.89	99.17	1.396	0.021
0.025	1.402	16.90	99.17	1.399	0.025
0.032	1.406	16.92	99.17	1.403	0.032
0.041	1.411	16.93	99.17	1.408	0.039
0.051	1.418	16.95	99.16	1.415	0.050
0.064	1.427	16.97	99.16	1.424	0.063
0.080	1.438	16.98	99.16	1.435	0.081
0.101	1.452	17.00	99.16	1.449	0.103
0.128	1.468	17.02	99.15	1.466	0.129
0.161	1.487	17.03	99.15	1.485	0.161
0.201	1.509	17.05	99.15	1.506	0.200
0.254	1.536	17.07	99.15	1.534	0.254
0.319	1.565	17.08	99.15	1.563	0.318
0.401	1.597	17.11	99.15	1.595	0.400
0.511	1.635	17.12	99.15	1.633	0.512

Table (4) shows the chosen calibration data that were done using the DANTEC calibrator. The calibrator successfully achieved the points of the chosen interval, although it struggled to achieve low velocities 0.02 m/s for example, but after some iterations that was achieved. The pressure of the outlet was almost constant as well as for the temperature, which helps having more accurate results. Figure (23) illustrates the calibration curve that was used to proceed in the measurement for the first part.

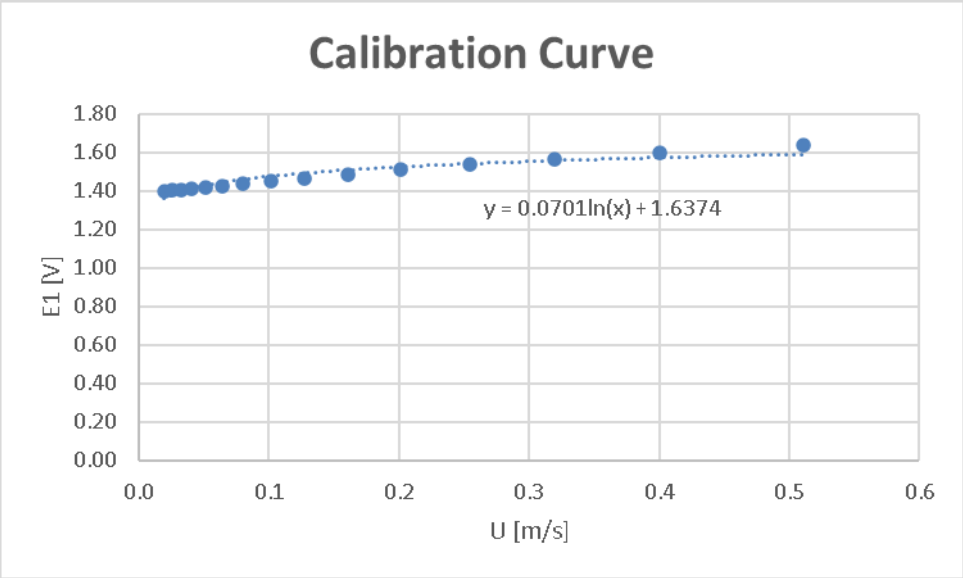

Figure 23. DANTEC Calibration curve 15.03.2022

A pre-set velocity is done to measure with the calibrated hot-wire, although we cannot validate how accurate are the velocity set by the DANTEC calibrator, it was assumed as a reference and the readings in Table (5) were compared to these values. Note that the readings are average velocities since the device reads 512 points at a time and gives the results. To validate that it'll read the same reading and no need for 10 points measurements for each velocity set, a random repeating for different points and the CTA gave the same reading multiple times, some exceptions appeared but with small deviation, for the purposes of this thesis it was decided that we attempt one measurement per point.

Table 5. Readings of DANTEC after calibration 15.03.2022

Uset [m/s]	Uavg [m/s]	Error [%]
0.020	0.024	18.09
0.050	0.051	0.96
0.101	0.103	1.68
0.127	0.127	0.16
0.153	0.153	0.33
0.177	0.175	1.35
0.204	0.200	1.82
0.252	0.246	2.34
0.300	0.293	2.33
0.354	0.344	2.93
0.400	0.388	3.00
0.447	0.435	2.73

0.500	0.487	2.64

The way of percent error calculation is explained in calculation's section.

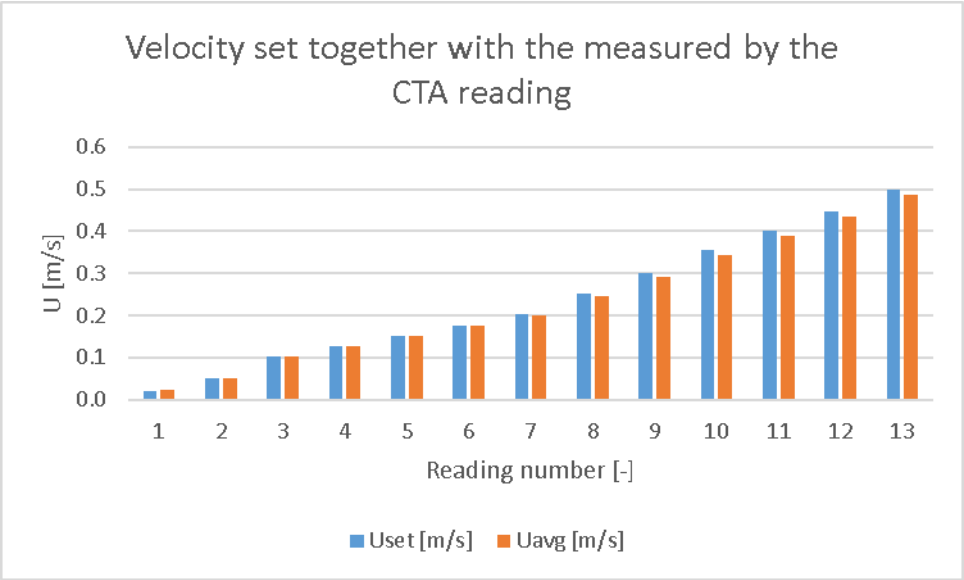

Figure 24. Set velocity vs measured velocity 15.03.2022

Figure (24) illustrates the results that were obtained using the calibration from DANTEC. It's clear that the calibration is well done, and the measured value is very close to the set value. The results also follow the fact that for a 0 m/s flow there is no reading. In the following figure (25) a plot for each reading with the percent error is done. The highest error was in the lowest velocity of the interval which was expected since the hot wire for such low velocity can be affected with more variables that in faster flows are neglected such as the effect of the signal interference and the resistance of the wires etc.

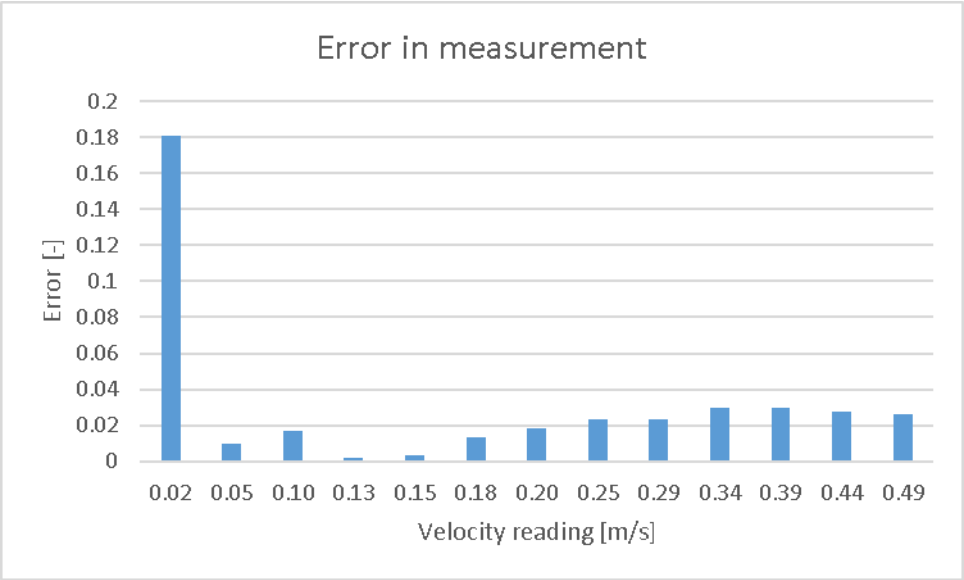

Figure 25. Error in measurements 15.03.2022

3.2 MEASUREMENT WITH THE NEW CALIBRATOR

With the new design we had to calibrate it before any measurement, the calibration data that we achieved are in table (6). The calibration curve is suggested to be logarithmic. The flowmeter as well as the flow itself had some fluctuations that's why the plotting of the data in figure (26) has deviation and doesn't line-up on the logarithmic line. We repeated the calibration several times and these data are the one that we chose as the best calibration points, since the logarithmic graph was obtained, and the deviation compared to the fluctuations are acceptable. Later will be explained some source of the fluctuations.

Table 6. Calibration data from HWC 1M 12.04.2022

Uaxial [m/s]	E1 [V]	T(C)	P(kPa)	E1corr [V]	U1calc [m/s]
0.029	1.387	17.00	99.29	1.385	0.029
0.038	1.406	17.00	99.39	1.404	0.041
0.047	1.416	16.90	99.50	1.413	0.047
0.047	1.412	17.00	99.50	1.410	0.045
0.058	1.429	16.90	99.69	1.426	0.057
0.062	1.435	16.80	99.76	1.431	0.062
0.078	1.455	16.80	100.10	1.451	0.078
0.084	1.462	16.70	100.25	1.457	0.084

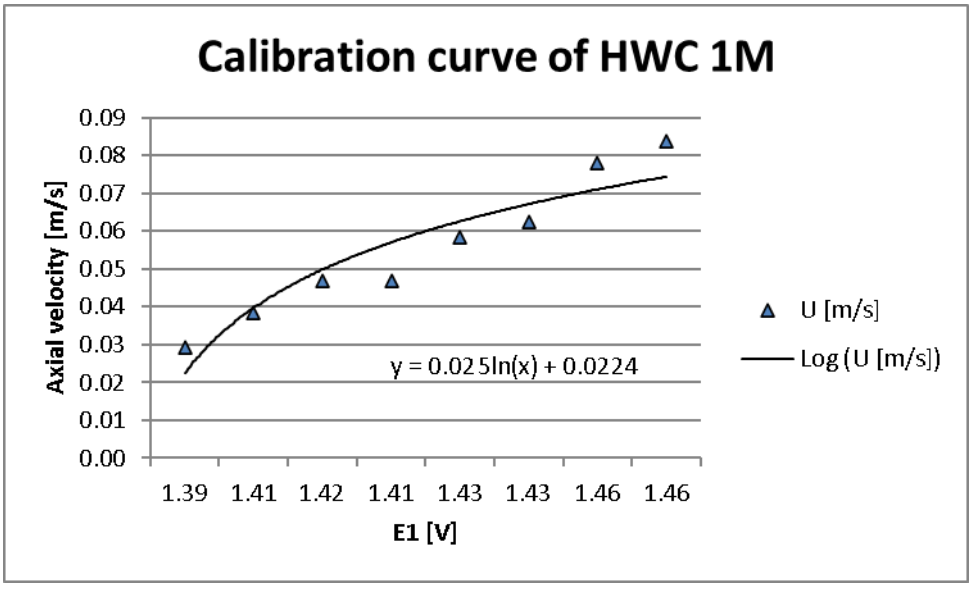

Figure 26. Calibration curve of HWC 1M 12.04.2022

As it was mentioned earlier in the methodology the profile should also be measured to obtain the correction factor. It was decided to choose a flowrate that can be easily achieved with the least fluctuations. The first flowrate was 22.95 L/min. The reading from the hotwire is illustrated in table (7). The profile coefficient that was obtained for such flow is

1.26. The way to calculate the profile coefficient is by calculating the average velocity of the measured values, divide the maximum velocity in the profile on the average that we got.

Table 7. Profile measurement FR 22.95 L/min, k = 1.26

z [cm]	velocity [m/s]
10	0.0288
9	0.0433
8	0.0482
7	0.0495
6	0.0473
5	0.0445
4	0.0401
3	0.0333
2	0.0291
1	0.0287
U_{avg}	0.0393

Figure (27) illustrates the profile of the flow at 22.95 L/min. The flow was expected to be in the laminar region of the flow, and a honeycomb and a strainer were added to smooth the flow more. As it was mentioned earlier the low velocity is affected by many variables that normally they're neglected.

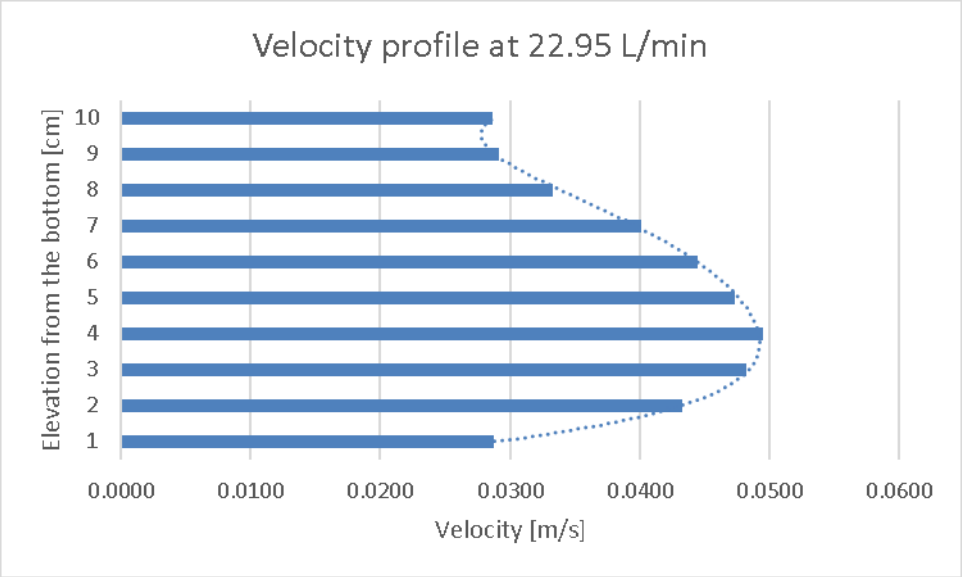

Figure 27. Velocity profile at 22.95 L/min

The same procedure of measurement was done for a different flowrate. It was chosen the flow of 31.80 L/min since it's less fluctuating than other flowrates in the range. The reading is illustrated in table (8). It was expected to also have a laminar flow character. Since this flowrate is higher, that means Reynold number is going to be higher, and the flow will be more turbulent like than the previous measured one. Figure (28) illustrates the

behaviour of the flow. The bigger the Reynold's number the smaller profile coefficient for the flow, the more turbulent the flow is. It was obtained in this case, the profile coefficient for this flowrate was 1.20 in comparison with 1.26 for the slower flow. The profile looks less steep than the previous which meets our expectations, but net steep enough to look like turbulent.

Table 8. profile measurement at 31.80 L/min, k = 1.20

z [cm]	velocity [m/s]
10	0.0287
9	0.0507
8	0.0594
7	0.0615
6	0.0601
5	0.0596
4	0.0592
3	0.0561
2	0.0469
1	0.0291
U_{avg}	0.0511

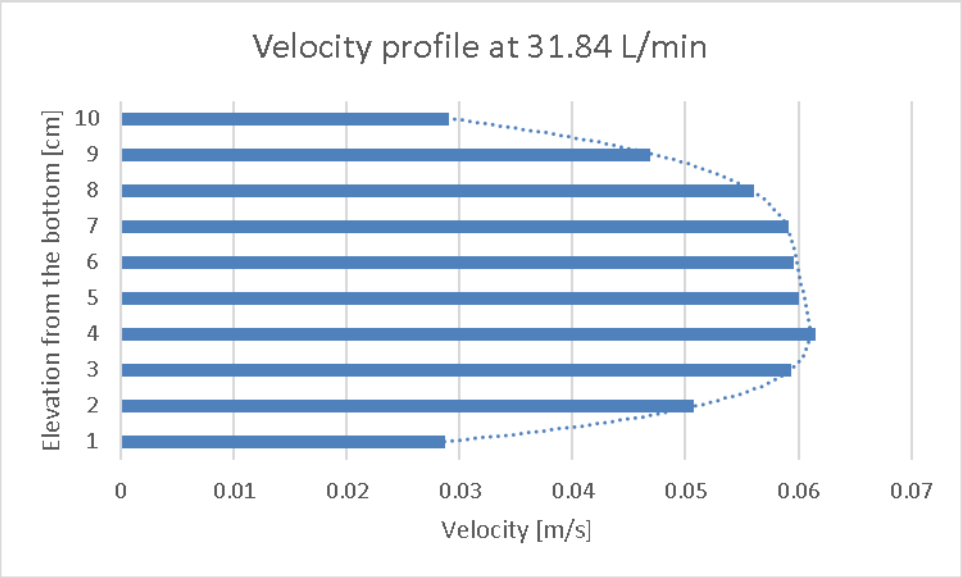

Figure 28. Velocity profile at 31.84 L/min

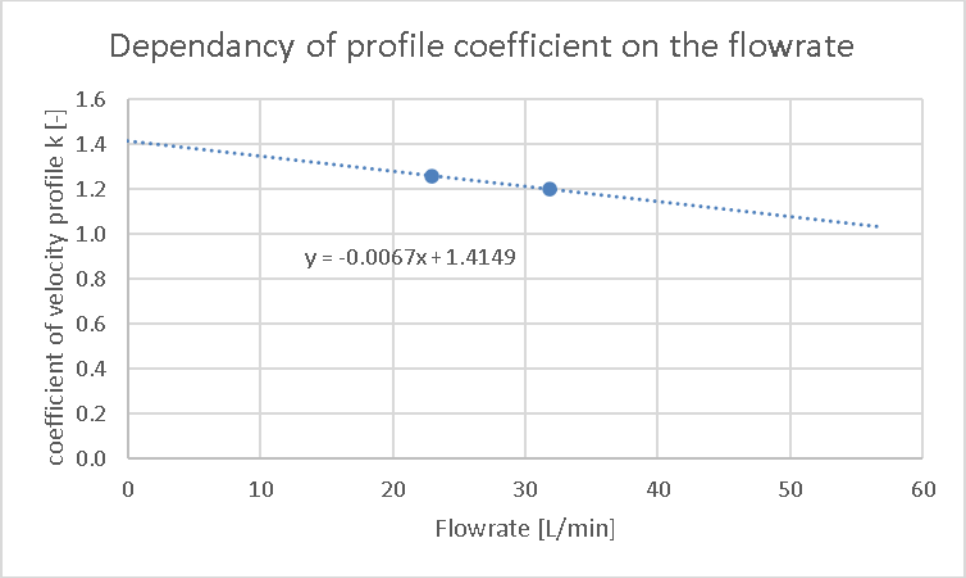

Figure 29. Dependence of profile coefficient on the flowrate

In this thesis the profile coefficient was taken for only 2 flowrates and from the plotted graph figure (29) the equation of the profile coefficient as a function of flowrate. It's recommended to measure the profile coefficient for more points for more accurate results, but for the purpose of this thesis it was decided that 2 points are enough. The main source of fluctuations in the flowrate is the source (the compressor) itself, for that reason we highly recommend using flow controller or any other equipment that can fulfil that purpose since the compressor won't give a stable flow. Table (9) shows the readings that were obtained from the measurement after the calibration with the new calibrator. The profile coefficient for each flow was calculated and multiplied with calculated the surface averaged velocity to get the actual velocity.

Table 9. Readings and calculation of the flow in the HWC 1M

Volumetric flow rate [L/min]	Diameter [m]	Area [m2]	Surface-averaged velocity [m/s]	Profile coefficient [-]	Axial velocity [m/s]	Measured velocity by CTA [m/s]	Deviation measured from calculated [%]
38.10	0.106	0.0088	0.0720	1.16	0.083	0.062	25.22
51.50	0.106	0.0088	0.0973	1.07	0.104	0.085	18.32
57.35	0.106	0.0088	0.1083	1.03	0.112	0.099	11.76
59.06	0.106	0.0088	0.1115	1.02	0.114	0.101	11.16
60.65	0.106	0.0088	0.1145	1.01	0.116	0.105	9.11
61.77	0.106	0.0088	0.1167	1.00	0.117	0.107	8.38

The actual velocity is compared with the measured velocity from the CTA by a percent error as shown in figure (30). As it was expected the highest percent error was with the lowest velocity, the higher the velocity the smaller the percent error, as it was mentioned previously more effects related to low velocities that's why the percent error is higher. Figure (31) shows both velocities together (the readings and the actual velocity).

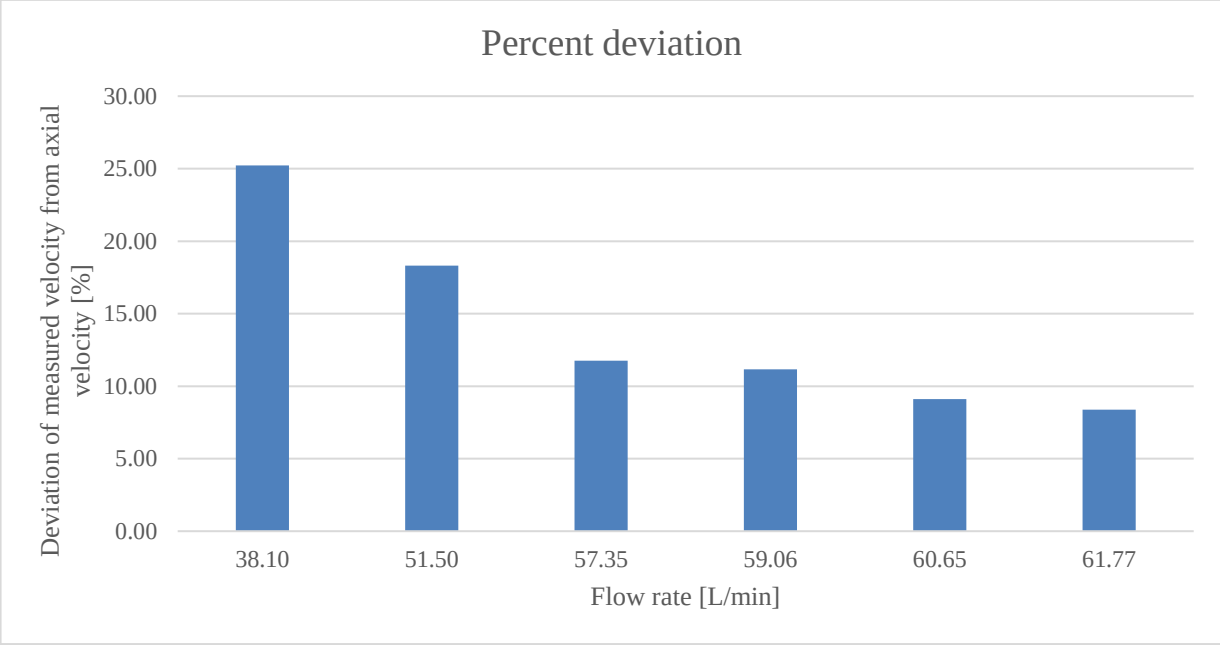

Figure 30. Percent error of the CTA reading with HWC 1M

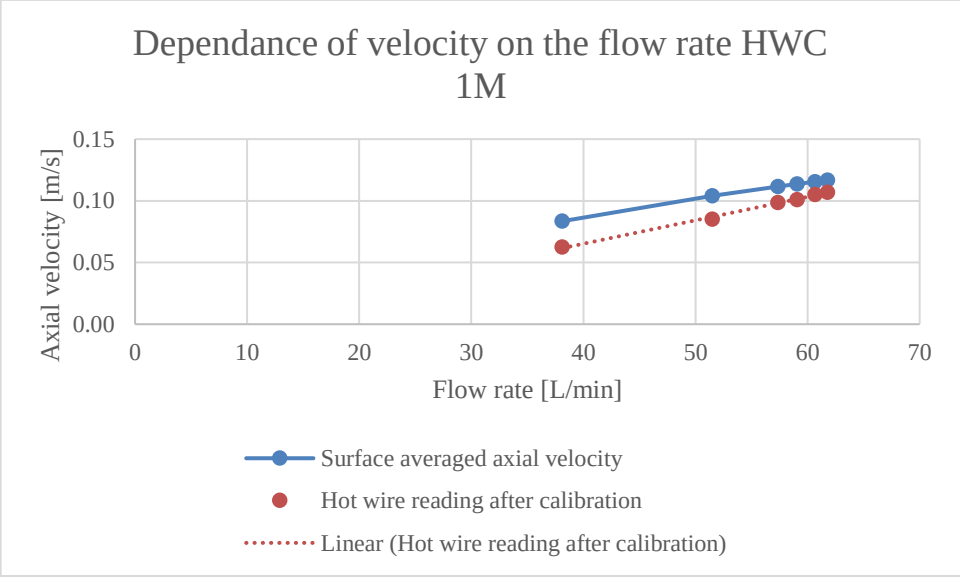

Figure 31. Surface averaged axial & measured velocities plotting against flowrate

The readings of the flow were less than 10 since we were limited by the valve limitation and the nature of the flow from the valve since it struggled to give us a stable flow with no fluctuations. The CTA wasn't able also to read more than 2 profiles on the same calibration since for some unknown reason the hot wire during the third time of measuring the profile started to give irrelevant readings. So, we tried to calibrate it again. The deviation that we've got between the readings and the actual velocities can be due to many reasons one of which is the losses that we neglect.

3.3 CALCULATIONS:

Reynold's number:

$Re = \rho \cdot U \cdot d/\mu$, where ρ is the density of the fluid, d is the diameter of the pipe, μ dynamic viscosity of the fluid, U is the velocity of the fluid.

$$\text{For 22.95 L/min} \ldots Re = \frac{0.043 \cdot 0.106 \cdot 1.204}{1.825 \cdot 10^{-5}} = 303 < 2000 \text{ Laminar flow}$$

Volumetric flowrate:

$$Q[m^3/s] = Q[L/min] \cdot 1\ m^3/1000\ L \cdot 60\ s/1\ min = 38.10 \cdot 60/1000 = 6.35 \cdot 10^{-4}\ m^3/s$$

Surface averaged velocity:

$$U_{SA}[m/s] = Q[m^3/s]/A[m^2] = \frac{0.000635 \cdot [m^3/s]}{0.0088247 \cdot [m^2]} = 0.07196\ m/s$$

Percent error:

$$percent\ error\ [\%] = (U_{SA} - U_m)/U_{SA} \cdot 100\% = (0.07196 - 0.0624)/0.07196 \cdot 100\% = 13.28\%$$

Correction factor:

$$k = \frac{U_{max}}{U_{avg}} = \frac{0.0596}{0.0511} = 1.20$$

3.4 MEASUREMENT WITH LDA

The results of the LDA are shown in table (10), and those readings are plotted in figure (32). There was a deviation of the readings from the LDA with the actual velocities, and some questions were asked after this: why the readings don't give a line that crosses the origin? why the deviation was increasing with the increasing of the flow velocity? To answer the first question, we had to go back to the experimental setup and check if everything was set correctly and the readings had a good reliability. All the readings expect for the 50 L/min had enough number of particles measured and they gave a linear trendline with small variations. Even the point that we would suspect it (50 L/min), complied with the trendline so it was believed to be correct for some extent but with less reliability. So, the readings are reliable for some extent. The next step was to check if the way the particles were introduced is the reason. If so, then the readings should be lower than the actual, so most probably the effect of the smoke at the end affected the flow but as a small effect that can be neglected in this scenario. Finally, we can suggest that such deviation was caused by an uncalibrated flowmeter. That can explain why the line is shifted and does not cross the origin. Also, that can explain why the actual velocity line has a different slope than the LDA readings line. If we consider the readings from the LDA are correct, then the flowrate where the line has velocity equals 0 m/s (around 29 L/min) is the offset of the flowmeter and should be calibrated again. Some of that graph behaviour can also be related to the flowmeter, due to unstable error with the flowmeter, that means with lower velocities it was able to measure the flowrate more accurate than when increasing the flowrate of the flow.

Table 10. LDA reading and some results

Volumetric flowrate [L/min]	Surface-averaged velocity [m/s]	Profile coefficient [-]	Actual velocity in the axis [m/s]	Measured velocity [m/s]	Deviation measured from calculated [%]
60	0.113	1.01	0.115	0.22	94.14
55	0.104	1.05	0.109	0.19	82.91
53	0.100	1.06	0.106	0.18	79.82
50	0.094	1.08	0.102	0.15	58.85
45	0.085	1.11	0.095	0.12	41.20
40	0.076	1.15	0.087	0.08	5.90

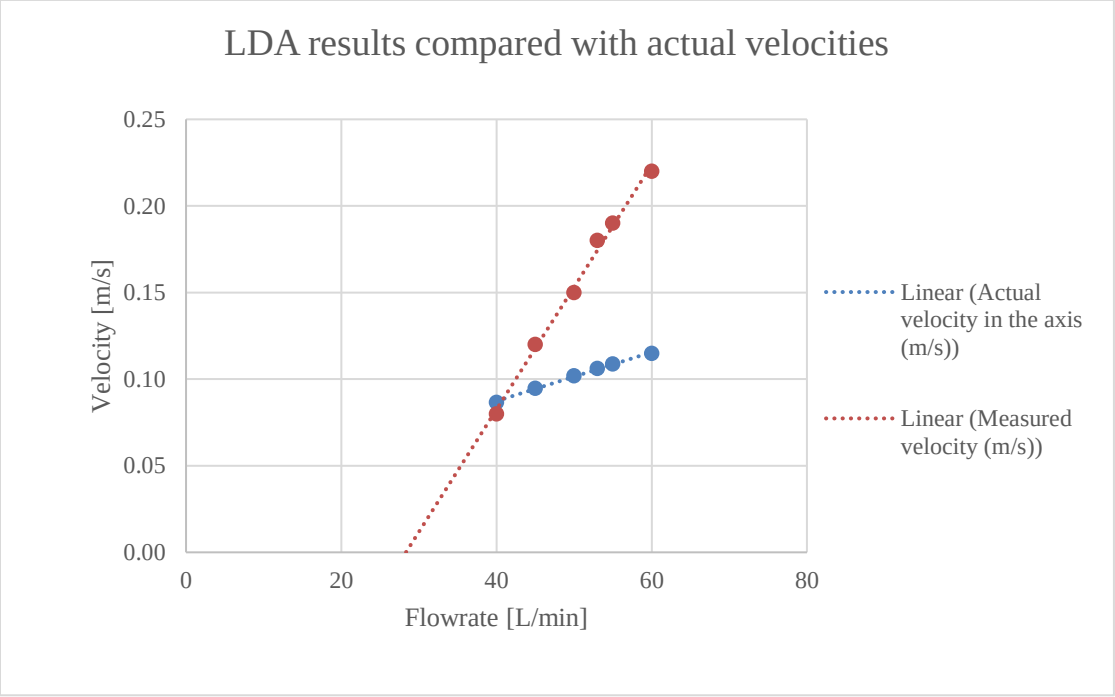

Figure 32. LDA results compared with actual velocities

4 CONCLUSION

In this thesis, which was focused on low velocity measurement using hot wire, measurement had taken place and to get sufficient knowledge for this purpose some scientific research was done. Also, some ideas of the calibrator were inspired by the others' work that was mentioned in the introduction.

For the DANTEC calibration set, it was unclear how accurate is the flow measurement. It was considered that the airflow controller is accurate when setting the velocity, so the reading from the DANTEC set has reasonably accuracy for velocities above 0.05 m/s (as it was mentioned in the discussion), nevertheless we can advise performing the calibration before every measurement and for more than 10 points in a logarithmic calibration since it gave the most accurate readings out of it.

For our model, an acceptable result was obtained in the sense of many uncertainties (convection, geometrical and length losses that were mentioned in the discussion section) that were neglected for our research. The readings that we got, gave a linear relationship. The linear function almost approaches 0 m/s for the 0 L/min flow. When the readings are compared to the actual values it gives a deviation that corresponds to the correction factor (correction factor that was used to calculate axial velocity from the surface averaged velocity). The profile coefficient relation with the flowrate was reasonable to some extent since the high flow rates give a more turbulent profile which gives a profile coefficient near 1, and the slower the flow the bigger the profile coefficient is, it's due to the shape of each flow type. DANTEC calibrator is better and easier to use then the new designed calibrator, hence the goal of that calibrator is to provide a simple alternative and relatively cheaper method to calibrate the hot wire.

An attempt to measure the flow velocity using a laser Doppler anemometer to compare its results with the results that we got after calibrating it with the HWC 1M. Unfortunately, the readings from the LDA had some deviation for the reasons mentioned previously. There were some issues with smoke injection into the flow, since it was a low velocity flow, some phenomena was observed when the smoke was injected that most of the smoke particles dropped to the bottom of the pipe when injected after the filter, that can be explained by buoyancy forces, particles most probably have a higher density then air, and the velocity of the flow is lower than the settling velocity. In addition, the honeycomb together with the foam filter filtered most of the particles if injected behind them (which is the right way to do it) as it was mentioned previously. An intensive laser beam (stronger than what is usually used) was used to get accurate results. Since LDA lab and CTA lab are different and each has it is own valve control, we tried to generate the same flowrates in both experiments to compare the results with each other. Finally, upon the results that were obtained from the simple calibrator that was designed, it is a success and can calibrate the hot wire, although further study is recommended. It is advised to vary the diffuser output diameter and length to fulfil others' needs, for example, higher velocity readings. To measure using LDA with such a design the smoke can be injected directly into the inlet and to remove the honeycomb and the foam filter but that would alter the flow profile. The LDA measurement results are not correct, and the measurement should be repeated, and, in this thesis, there was not enough time to remeasure that.

REFERENCES

[1] LOMAS C G. Fundamentals of Hot Wire Anemometry. *Cambridge: Cambridge University Press*. 2011. ISSN 978-0-521-28318-2.

[2] PERRY A E. Hot-Wire Anemometry. *New York: Oxford University Press*. 1982. ISSN 978-0-198-56327-3.

[3] MIRHASHEMI, Arman, Joshua D SZCZUDLAK a Scott C MORRIS. Hot-wire probe design and calibration for high-speed, high-temperature flows. *Measurement Science and Technology* [online]. 2021, **32**(4), 400-404 [cit. 2022-05-10]. ISSN 0957-0233. Available: doi:10.1088/1361-6501/abcefc

[4] COMTE-BELLOT, G, Joshua D SZCZUDLAK a Scott C MORRIS. Hot-Wire Anemometry. *Annual Review of Fluid Mechanics* [online]. 1976, **8**(1), 209-231 [cit. 2022-05-10]. ISSN 0066-4189. Available: doi:10.1146/annurev.fl.08.010176.001233

[5] TAKAHASHI, Hidemi, Mitsuru KURITA, Hidetoshi IIJIMA a Seigo KOGA. Simplified Calibration Method for Constant-Temperature Hot-Wire Anemometry. *Applied Sciences* [online]. 2020, **10**(24), 209-231 [cit. 2022-05-10]. ISSN 2076-3417. Available: doi:10.3390/app10249058

[6] BRUUN H. 1996. Hot-Wire Anemometry: Principles and Signal Analysis. *Oxford science publications*, ISBN 433-7-94243-6.

[7] PERSOONS, Tim, Ad HOEFNAGELS, Eric VAN DEN BULCK a Seigo KOGA. Calibration of an oscillating hot-wire anemometer for bidirectional velocity measurements. *Experiments in Fluids* [online]. 2006, **40**(4), 555-567 [cit. 2022-05-10]. ISSN 0723-4864. Available: doi:10.1007/s00348-005-0095-4

[8] LIGRANI, P M, R V WESTPHAL, F R LEMOS a Seigo KOGA. Fabrication and testing of subminiature multi-sensor hot-wire probes. *Journal of Physics E: Scientific Instruments* [online]. 1989, **22**(4), 262-268 [cit. 2022-05-10]. ISSN 0022-3735. Available: doi:10.1088/0022-3735/22/4/011

[9] YASA, T., G. PANIAGUA, R. DÉNOS a Seigo KOGA. Application of Hot-Wire Anemometry in a Blow-Down Turbine Facility. *Journal of Engineering for Gas Turbines and Power* [online]. 2007, **129**(2), 420-427 [cit. 2022-05-10]. ISSN 0742-4795. Available: doi:10.1115/1.2364191

[10] INASAWA, Ayumu, Shohei TAKAGI, Masahito ASAI a Seigo KOGA. Improvement of the signal-to-noise ratio of the constant-temperature hot-wire anemometer using the transfer function. *Measurement Science and Technology* [online]. 2020, **31**(5), 420-427 [cit. 2022-05-10]. ISSN 0957-0233. Available: doi:10.1088/1361-6501/ab6916

[11] SUBRAMANIYAM, S., V. GANESAN, P. Srinivasa RAO a S. SAMPATH. Turbulent flow inside the cylinder of a Diesel engine — an experimental investigation using hot wire anemometer. *Experiments in Fluids* [online]. 1990, **9**(3), 167-174 [cit. 2022-05-10]. ISSN 0723-4864. Available: doi:10.1007/BF00187418

[12] LEE, T, R BUDWIG, P. Srinivasa RAO a S. SAMPATH. Two improved methods for low-speed hot-wire calibration. *Measurement Science and Technology* [online]. 1991, **2**(7), 643-646 [cit. 2022-05-10]. ISSN 0957-0233. Available: doi:10.1088/0957-0233/2/7/011

[13] ÖZAHI, Emrah, Melda Özdinç ÇARPINLIOĞLU, Mehmet Yaşar GÜNDOĞDU a S. SAMPATH. Simple methods for low speed calibration of hot-wire anemometers. *Flow Measurement and Instrumentation* [online]. 2010, **21**(2), 166-170 [cit. 2022-05-10]. ISSN 09555986. Available: doi:10.1016/j.flowmeasinst.2010.02.004

[14] KOHAN, S., Melda Özdinç ÇARPINLIOĞLU, Mehmet Yaşar GÜNDOĞDU a S. SAMPATH. Low speed calibration formula for vortex shedding from cylinders. *Physics of Fluids* [online]. 1973, **16**(9), 166-170 [cit. 2022-05-10]. ISSN 00319171. Available: doi:10.1063/1.1694554

[15] Roshko, A., On the development of turbulent wakes from vortex streets. *NACA-TR-1191*. 1954.

[16] CHRISTMAN, P J, J PODZIMEK, Mehmet Yaşar GÜNDOĞDU a S. SAMPATH. Hot-wire anemometer behaviour in low velocity air flow. *Journal of Physics E: Scientific Instruments* [online]. 1981, **14**(1), 46-51 [cit. 2022-05-10]. ISSN 0022-3735. Available: doi:10.1088/0022-3735/14/1/013

[17] Aydin, M. and Leutheusser, H.J. Very low velocity calibration and application of hot-wire probes. *DISA information*. 1980.

[18] TSANIS I K. Calibration of hot-wire anemometers at very low velocities. *Toronto University, Canada*.1987.

[19] BRUUN, H. H., B. FARRAR, I. WATSON a S. SAMPATH. A swinging arm calibration method for low velocity hot-wire probe calibration. *Experiments in Fluids* [online]. 1989, **7**(6), 400-404 [cit. 2022-05-10]. ISSN 0723-4864. Available: doi:10.1007/BF00193422

[20] GUELLOUZ, M. S., S. TAVOULARIS, I. WATSON a S. SAMPATH. A simple pendulum technique for the calibration of hot-wire anemometers over low-velocity ranges. *Experiments in Fluids* [online]. 1995, **18**(3), 199-203 [cit. 2022-05-10]. ISSN 0723-4864. Available: doi:10.1007/BF00230265

[21] YUE, Zou, Tor G MALMSTRÖM, Mehmet Yaşar GÜNDOĞDU a S. SAMPATH. A simple method for low-speed hot-wire anemometer calibration. *Measurement Science and Technology* [online]. 1998, **9**(9), 1506-1510 [cit. 2022-05-10]. ISSN 0957-0233. Available: doi:10.1088/0957-0233/9/9/020

[22] JOHNSTONE, Andrew, Mesbah UDDIN, Andrew POLLARD a S. SAMPATH. Calibration of hot-wire probes using non-uniform mean velocity profiles. *Experiments in Fluids* [online]. 2005, **39**(3), 527-534 [cit. 2022-05-10]. ISSN 0723-4864. Available: doi:10.1007/s00348-005-0972-x

[23] AL-GARNI, Abdullah M., Mesbah UDDIN, Andrew POLLARD a S. SAMPATH. Low speed calibration of hot-wire anemometers. *Flow Measurement and Instrumentation* [online]. 2007, **18**(2), 95-98 [cit. 2022-05-10]. ISSN 09555986. Available: doi:10.1016/j.flowmeasinst.2007.01.003

[24] TRITTON, D. J., Mesbah UDDIN, Andrew POLLARD a S. SAMPATH. Experiments on the flow past a circular cylinder at low Reynolds numbers. *Journal of Fluid Mechanics* [online]. 1959, **6**(4), 547-567 [cit. 2022-05-10]. ISSN 0022-1120. Available: doi:10.1017/S0022112059000829

[25] GERRARD, J. H., Mesbah UDDIN, Andrew POLLARD a S. SAMPATH. The mechanics of the formation region of vortices behind bluff bodies. *Journal of Fluid Mechanics* [online]. 1966, **25**(2), 401-413 [cit. 2022-05-10]. ISSN 0022-1120. Available: doi:10.1017/S0022112066001721

[26] WEBSTER, C. A. G., Mesbah UDDIN, Andrew POLLARD a S. SAMPATH. An experimental study of turbulence in a density-stratified shear flow. *Journal of Fluid Mechanics* [online]. Berlin, Heidelberg: Springer Berlin Heidelberg, 1964, 1988, **19**(02), 595-608 [cit. 2022-05-10]. ISBN 978-3-642-73693-3. ISSN 0022-1120. Available: doi:10.1017/S0022112064000672

[27] COLLIS D AND WILLIAMS J. 1959. *Two-dimensional convection from heated wires at low Reynolds numbers.*

[28] NĚMEČEK P. Nejistoty měření. *Praha: Česká společnost pro jakost, Kvalita, quality, Qualität.* 2008. ISBN 978-80-02-02089-9.

[29] GOODFELLOW, Howard a Esko TAHTI. *Industrial Ventilation Design Guidebook* [online]. 2001 [cit. 2022-05-10]. Available: doi:10.1016/B978-0-12-289676-7.X5000-0

[30] JENSEN, K. D. Flow measurements. *Journal of the Brazilian Society of Mechanical Sciences and Engineering* [online]. 2004, **26**(4) [cit. 2022-05-10]. ISSN 1678-5878. Available: doi:10.1590/S1678-58782004000400006

[31] MiniCTA and Multichannel CTA: Compact CTA Systems for accurate flow investigations [online]. *DANTEC DYNAMICS*, 2020. Available: https://www.dantecdynamics.com/wp-content/uploads/2020/03/0560_v1-1_SS-MiniCTA-Multichannel-CTA-systems.pdf

LIST OF ATTACHMENTS

I. Designed HWC 1M
II. CTA data
III. LDA data